Partial ionization in dense plasmas: Comparisons among average-atom density functional models

Michael S. Murillo, Jon Weisheit, Stephanie B. Hansen, and M. W. C. Dharma-wardana

Phys. Rev. E **87**, 063113 — Published 28 June 2013

DOI: 10.1103/PhysRevE.87.063113

Partial Ionization in Dense Plasmas: Comparisons Among Average-Atom Density Functional Models

Michael S. Murillo
*Computational Physics and Methods Group, Los Alamos National Laboratory, Los Alamos, NM 87545**

Jon Weisheit
Department of Physics & Astronomy, University of Pittsburgh, Pittsburgh, PA 15260

Stephanie B. Hansen
Lawrence Livermore National Laboratory, Livermore, CA 94550
Sandia National Laboratory, Albuquerque, NM 87185

M. W. C. Dharma-wardana
Institute of Microstructural Sciences National Research Council of Canada, Ottawa, Canada K1A 0R6

Nuclei interacting with electrons in dense plasmas acquire electronic bound states, modify continuum states, generate resonances and hopping electron states, and generate short-range ionic order. The mean ionization state (MIS), i.e, the mean charge Z of an "average ion" in such plasmas is a valuable concept: pseudo-potentials, pair-distribution functions, equations of state, transport properties, energy-relaxation rates, opacity, radiative processes, etc., can all be formulated using the MIS of the plasma more concisely than with an "all-electron" description. However, the MIS does not have a unique definition and is used and defined differently in different statistical models of plasmas. Here, using the MIS formulations of several average-atom models based on density functional theory, we compare numerical results for Be, Al, and Cu plasmas for conditions inclusive of incomplete atomic ionization and partial electron degeneracy. By contrasting modern orbital-based models with orbital-free Thomas-Fermi models, we quantify effects of shell structure, continuum resonances, the role of exchange and correlation, and the effects of different choices of the fundamental cell and boundary conditions. Finally, the role of the MIS in plasma applications is illustrated in the context of X-ray Thomson scattering in warm dense matter.

PACS numbers: 52.25.Jm, 61.05.cf, 71.15.Mb, 52.27.Gr

I. INTRODUCTION

The ionization state of elements at a given compression and temperature is an important quantity in plasma physics and material science. Some applications, such as the analysis of spectral line shapes, require detailed information about charge state distributions and their time dependent fluctuations [1, 2]. However, a large class of properties depends only on average values of certain basic plasma properties. Thermodynamic properties, linear transport, and optical properties serve as examples. A parameter which has proven to be invaluable, especially in models where the plasma is treated as a collection of charged point ions and electrons is the mean ionization state (MIS) Z of the ions (here we take the electron charge as $|e|$=1, and we use Hartree atomic units when convenient). Thus, if the number of ions per unit volume is n_i, the number of "free" electrons per unit volume in the plasma, viz., $n_e = Zn_i$. Basic calculations of equation of state and transport properties require only n_e or the average charge Z of ionic scattering centers. For example, only low-order moments of the charge state distribution appear in elementary formulae for the pressure of a dilute plasma, X-ray Thomson scattering cross sections, bremsstrahlung, electrical resistivity, and the electron-ion temperature relaxation rate [3–7]. In regimes where the point-ion model fails, the mean ionization enters as an essential parameter of pseudopotentials with finite core sizes used in quantum calculations [8, 9].

For weakly interacting plasmas (low densities and high temperatures), composition fractions X_i of an element's ionization states Z_i can be obtained from the Saha equation [1, 4], which is based on a balance of free energies of ideal gases. However, the ideal gas partition function is not convergent unless the sums are restricted to a finite number of states via a physically motivated cut off. Extending the Saha equation's regime of validity to strongly coupled plasmas (dense, partially degenerate plaasmas or low-density, low-temperature plasmas) in which Rydberg states and continuum states are occupied requires the formulation of convergent partition functions by including many-body effects that set natural bounds to the extent of the density of states. Generalized Saha equations, which incorporate some phenomenological modification of energy spectra and the density of states are used in the so-called "chemical picture" [10]; an example is the Hummer and Mihalas scheme that uses the plasma microfield to reduce occupation probabilities [11]. Astro-

*Electronic address: murillo@lanl.gov

physical opacity predictions using that model were found to be incorrect, however, as shown by Iglesias and Rogers [12].

Such phenomenological Saha schemes are unreliable and fail at strong coupling. Then a "physical picture" [8, 10, 13, 14] that views the plasma as a collection of nuclei and electrons supporting delocalized and localized states is needed. Activity expansions for effective composite particles [13] and models based on self-consistent-field calculations (mean-field approximations) for confined atoms [15] have been used to treat partially ionized atoms of differing charge states. Another class of physical picture models[16, 17] considers the mean ionization of a representative "average atom" (AA), viz., a spherical cell of plasma centered on one nucleus, instead of the distribution of actual charge states. A single determinant is used for the electronic wavefunction. An "average molecule" involving many ionic centers may also be used used in the calculation, as done in ab initio molecular dynamics (AIMD) schemes. But the extension to several determinants (configuration interaction), is currently computationally intractable. The method of Ref. [8] is a direct generalization of [16, 17] to include a co-existing multiplicity of species of charge states, using density functional theory (DFT) [18, 19] to calculate the free energies, EOS and transport coefficients within a fully physical approach. This method avoids the assumption of a single-determinantal model with a single average $\langle Z \rangle$ used in the average-atom model. We will not address all these alternatives fully, but only to the extent of their relevance to alternative definitions of MIS and leading to differing values of Z.

Density functional theory (DFT) [20, 21] is the languge that most average-atom models are based on, according to which *all equilibrium plasma properties* such as internal energy, pressure and entropy can be described as functionals of the *total* electron density $n_e(\mathbf{r})$ and the density $n_i(\mathbf{r})$ of the nuclei. Thus the MIS, defined as the mean charge Z of an ion, would also be a functional of $n_e(\mathbf{r})$ and $n_i(\mathbf{r})$. Then, incorporating Z in pseudopotentials, a simplified DFT which need not deal with the bound electrons of the core can be constructed, as is often done in practice for $T = 0$ problems. From then on, we need not deal with the bound electrons, and the electron density $n_e(\mathbf{r})$ now refers only to the free-electron density, with average densities satisfying $n_e = Zn_i$. Thus, the use of the MIS simplifies calculations of equilibrium properties as well as dynamical, non-equilibrium properties such as stopping of fast charges [5, 22], temperature relaxation [23, 24], or ion microfield fluctuations [25, 26]. The reason that such constructions are needed is simply that "all-electron" calculations are extremely costly in the context of time-dependent DFT [27, 28]) and other relevant methods. Similarly, the Kubo-Greenwood relations [29–31] can be used to calculate linear transport and optical properties either within an all-electron approach, or within a pseudo-potential approach assuming a well-defined core of electrons (thus specifying a MIS).

The goal of this work is to explore key MIS-related issues for AA models based on DFT. We employ models with spherical symmetry around a central nucleus, since we are interested in plasmas with temperatures that far exceed chemical bond energies associated with cluster formation.

A computationally more expensive alternative is to treat many nuclei in a periodic cell using either quantum Monte Carlo (QMC) or AIMD. Time dependence of the nuclei is included (in AIMD) on the Born-Oppenheimer surface generated by the electronic DFT calculation [32]. Here, we do not consider AIMD for three reasons. First, although the AIMD method can be generalized to finite temperatures, it has been computationally limited to lower temperatures ($T < 10$ eV) in practice. Second, most implementations [32] of AIMD employ for the core electrons a zero-temperature pseudopotential and a corresponding prescription for it. That is, the MIS is assumed and is not computed self-consistently with the bound and conduction electrons at finite T. Third, single center models are known to be quite accurate even for liquid metals, and we are not concerned with systems that form molecular species at very low temperatures that cannot be described by a single center. Orbital-free DFT (OFDFT) methods promise to remove many of these limitations [33–37], but little attention to the MIS has been given in them.

Methods which are in-between AA models and full-AIMD approaches also exist. These approaches include many correlated ions spherically averaged around one nucleus [39–42]. We do not consider these methods which are relatively less developed, especially in dealing with the MIS, which is our main focus. Furthermore, in regard to AIMD, all the thermodynamic results obtained by AIMD variants can be obtained very cheaply using the multi-species DFT method of Perrot et al. [8] where separate AA-like calculations for different ionization states of an element in a plasma are combined within an equation of state (EOS) to obtain the lowest energy composition fractions and the mean ionization.

We begin in Section II with an overview of plasma regimes, dimensionless parameters and their generalization using MIS definitions. In Section III we present the MIS as formulated in the three DFT-models we employ. Two are based on a single ion in a Wigner-Seitz cell. The third uses a single nucleus at the center, and many "field ions" contained in a cell (known as the *correlation sphere*, CS) which is at least a 100 times the volume of the Wigner-Seitz cell. This sphere encompasses the plasma volume within which ion-ion, ion-electron and electron-electron correlations die away. In Section IV, we present and contrast various MIS values computed by the different models for several metals, at densities bracketing normal solid density, and across a range of temperatures. In Section V, we consider implications of these results for X-ray Thomson scattering. Section VI provides a brief summary and future directions.

II. CHARACTERIZATION OF DENSE PLASMAS

Dense plasmas are usually characterized by dimensionless parameters (DP). Here, we display their dependence on the MIS charge Z. Strictly speaking, appropriate DP for plasmas arise naturally in the context of a given physical property [43, 44] where they are used as expansion parameters for corrections beyond a reference state, as in the Debye-Hückel theory for weak plasmas. Thus the strong-coupling plasma parameter Γ (see below) was initially used for expanding the free energy of the classical one-component plasma (OCP), until it was shown that such expansions are not really meaningful in strongly coupled regimes. Thus the use of these DP are mainly used now for qualitative characterizations of plasma conditions.

Often a MIS Z of ions in a plasma is estimated by a Thomas-Fermi-type theory, which serves to get dimensionless parameters that are useful in qualitative considerations [6, 43, 45]. We write these DP using a Z that relates the average ion density n_i to the average free electron density $n_e = Zn_i$, and evaluate the DP as a function of Z to reveal their ionization dependence. Note that the use of a MIS enables us to remove bound electrons from the problem, as they are subsumed in constructing Z. In the discussion that follows in this section, all electrons n_e are "free", i.e., delocalized.

The parameter Θ is a measure of the quantum degeneracy of the plasma electrons n_e, *viz.*,

$$\Theta = \frac{E_F}{T} = \frac{e^2 a_0}{2T} \left(3\pi^2 n_e\right)^{2/3}. \tag{1}$$

Here, T is the plasma temperature (in energy units), E_F is the usual Fermi energy defined in terms of the average density n_e of "free" electrons, and $(e^2/a_0) = 27.21$ eV is the atomic unit of energy. (More will be said about the precise definition of "free" in what follows, and in this section we use n_e to be a generic choice). When $\Theta \geq 1$ the plasma electrons are partially degenerate.

Another possible degeneracy parameter is $\eta_e = \mu_e/T$, where μ_e is the electron chemical potential for the fully, interacting system, including finite T-, finite density-, and bound state information not captured by (1). These modification of μ_e due to electron-ion interactions is sometimes loosely called the "lowering of the continuum". The parameter η_e plays a key role in the MIS-values predicted by DFT. For the homogeneous electron gas, when $\eta_e = 0$ then $\Theta = 1$ to within 1 percent. In the high density limit (at constant T), pressure ionization eliminates all bound states, and η_e approaches Θ. While a negative η is typical of uniform classical plasmas, note that this definition, which will be explored below, includes bound electrons.

The Coulomb coupling parameter is the ratio of the mean unscreened potential energy, estimated as the Coulomb energy of a pair of particles with charges $Z_\alpha e$ and $Z_\beta e$ at a separation $a_{\alpha\beta}$, to the mean kinetic energy, estimated classically as T, for a pair of particles α and β, or

$$\Gamma_{\alpha\beta} = \frac{Z_\alpha Z_\beta e^2}{a_{\alpha\beta} T} \tag{2}$$

$$a_{\alpha\alpha} = a_\alpha = (4\pi n_\alpha/3)^{-1/3} \tag{3}$$

$$a_{\alpha\beta} = (4\pi(n_\alpha + n_\beta)/3)^{-1/3}; \quad \alpha \neq \beta. \tag{4}$$

Thus $\alpha = i$, $a_i = (4\pi n_i/3)^{-1/3}$ is the Wigner-Seitz radius (WSR) of ions in a plasma with average ion density $n_i = n_e/Z$. The electron WSR is often denoted by r_s in condensed-matter physics. The Γ_{ee} defined in this traditional manner does not correctly reduce to r_s as $T \to 0$. The inter-pair length $a_{\alpha\beta}$ is a measure of the mean separation, and other definitions are also used. These Coulomb parameters satisfy the relations

$$\Gamma_{ii} = Z^{5/3}\Gamma_{ee} = \{Z/(1+Z)^{1/3}\}\Gamma_{ei}. \tag{5}$$

When $\Gamma_{\alpha\beta}$ exceeds unity, strong spatial correlations between particles of type α and type β, develop, and their pair distribution functions (PDF) deviate significantly from those of weak-coupling theory, showing oscillatory structures.

Because the electrons are polarized by the ions, the effective coupling between ions in plasmas tends to be smaller than the "bare" parameter of (2). Furthermore, in the domain of partial electron degeneracy, the effective couplings that involve electrons are also reduced, and one can (approximately) replace T by an effective temperature $\tilde{T}_e$ that goes to a $T_q = 2E_F/3$ at $T = 0$ and tends to T itself at very high temperature. A more rigorous approach is to use a "quantum temperature" T_q instead of $2E_F/3$, where the T_q is determined from a classical map of suitable quantum properties [46, 47]

$$\tilde{\Gamma}_{ei} = \frac{Ze^2}{a_{ei}\tilde{T}_e}; \;\; \tilde{T}_e = \sqrt{T^2 + T_q^2} \tag{6}$$

The use of the classical-map T_q in Γ_{ee} ensures that it reduces correctly to r_s at $T = 0$. For low temperature applications in classical maps near $T = 0$, the Coulomb interaction e^2/a_e itself has to be corrected for diffraction effects associated with the thermal de Broglie length of the electrons [46]. However, such corrections are not needed for the regimes used in the present study.

Using such an effective electron temperature in a screening length λ_s which depends on the density and $\tilde{T}_e$, an effective ion-ion coupling including screening can be given as:

$$\tilde{\Gamma}_{ii}^{scr} = \frac{Z^2 e^2}{a_i \tilde{T}_e} e^{-a_i/\lambda_s}. \tag{7}$$

This coupling parameter, which is always smaller than the "bare" Γ_{ii}, is a more realistic measure of the actual ionic coupling in Yukawa fluids. The numerical value of λ_s depends on the physical properties of the plasma under consideration, but a Thomas-Fermi form is typically used [48].

The plasmas studied in astrophysics, in the laboratory, or computationally, involve temperatures and densities which change by orders of magnitude as materials are heated, ionized, and forced into compression or allowed to expand {see Refs. [49–53] for several familiar examples}. Thus one needs the MIS Z over a wide variety of conditions, even to identify the regimes accessed by the plasma in terms of traditional plasma parameters; that is, the value of Z to be used in (2)-(7) is poorly known. Indeed, the large variations occurring in these MIS-dependent parameters highlight the difficulty of plasma theory for partially ionized, dense matter. We display the behavior of these dimensionless parameters as a function of the MIS Z.

In this study we focus on plasmas having just a single element of nuclear charge Z_{nuc}. We study Be, Al, and Cu, whose normal-solid mass densities are, respectively, $\rho_0 = 1.85, 2.70, 8.92$ g/cm^3. As an example of the complexity of even this simple case, the top panel of Fig. 1 shows contours of the MIS for Al over a large range of temperatures and relative compression ρ/ρ_0. The MIS is from More's fit [54] to the Thomas-Fermi MIS $\langle Z \rangle$, discussed in Section III C and given in (20), below. Note that greater ionization occurs both as the temperature increases and as the density increases above $\rho/\rho_0 \approx 1$, where pressure ionization begins. Fig. 1 also shows contours of Θ in the middle panel, where the continuum electrons in an Al plasma exhibit strong quantum effects at high density and low temperature. In the bottom panel of Fig. 1, contours of the modified electron-ion coupling parameter $\tilde{\Gamma}_{ei}$ are shown. Interestingly, the strongest electron-ion coupling occurs at low temperatures near normal solid density: higher densities decrease inter-particle separations but increase the effective temperature (introduced in (6)). Here, we see an interesting effect of the MIS, which occurs explicity in the factor Z and implicitly in both the mean separation a_{ei} and the effective temperature. We see that the electron-ion coupling is never very large because, if it were, the plasma would recombine to a lower MIS value, thereby decreasing the electron-ion coupling. That is, because (6) refers to *free* electron coupling to a composite ion of charge Z, Z has a complicated temperature and density dependence, here taken from the More fit. In Fig. 2, we plot contours of the bare ion-ion coupling parameter Γ_{ii}, again using (20) given below, for all three metals investigated here. Contours in these maps were chosen to reveal important modifications to standard formulae as the MIS varies with temperature and density. When this coupling is strong, correlations among ions produce oscillatory radial distributions at distances beyond a Wigner-Seitz radius. The effect of this on the plasma electronic structure is included in a statistical way in two-component correlation-sphere models, discussed in Sec. III E.

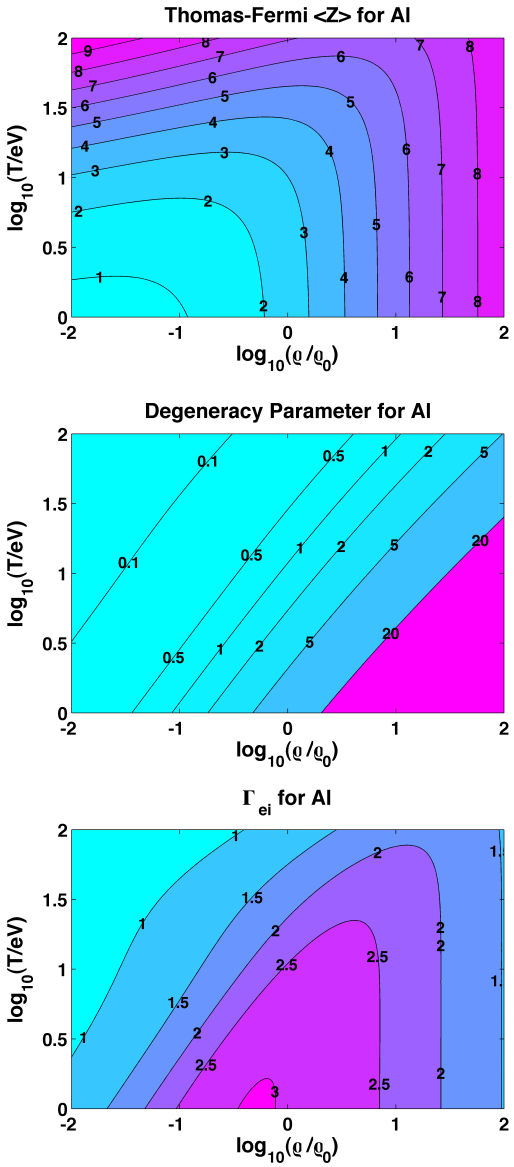

FIG. 1: (Color online) (top) Surface map of the Thomas-Fermi $\langle Z \rangle$ for Al as a function of temperature and relative density ρ/ρ_0. (center) Surface map of Θ, measuring quantum effects, for electrons in Al plasma, computed using the result from the top panel. (Bottom) Surface map of electron-ion coupling parameter for Al plasma computed using result from the top panel.

III. FINITE-TEMPERATURE DENSITY FUNCTIONAL MODELS AND MEAN IONIZATION STATE DEFINITIONS

This section describes two distinct kinds of statistical models based on DFT. Comprehensive accounts of DFT concepts are widely available [20, 21, 32, 55], while the review by Dharma-wardana and Perrot in Gross et al. [20] is specifically directed to electron-ion plasmas.

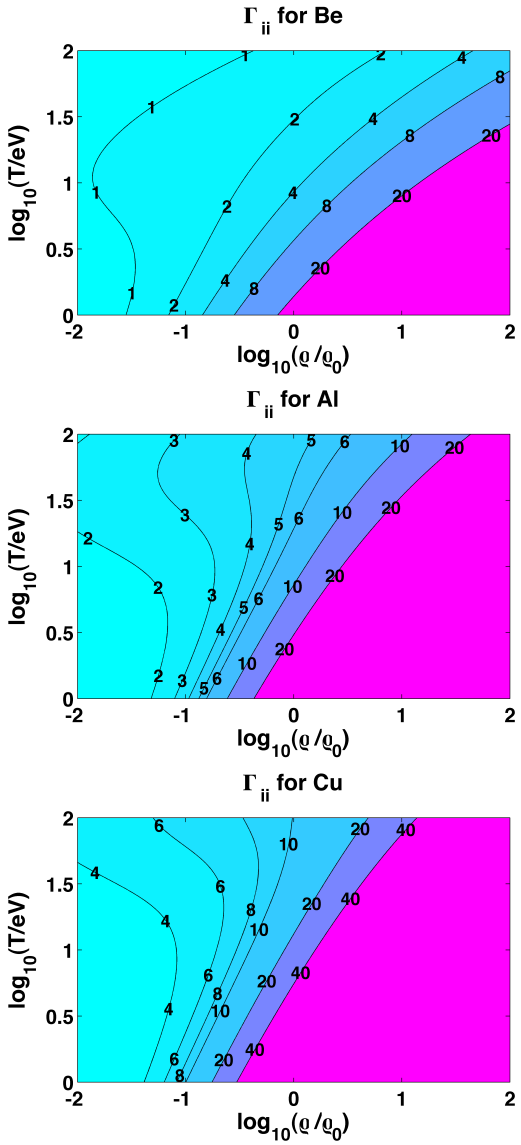

FIG. 2: (Color online) (top) Surface map of ion-ion coupling parameter for Be. (center) Surface map of ion-ion coupling parameter for Al. (bottom) Surface map of ion-ion coupling parameter for Cu. In all cases, the TF $\langle Z\rangle$ definition of (20) was used.

A. Ion-Sphere and Correlation-Sphere Models

In both ion-sphere (IS) and correlation sphere (CS) models one nucleus is fixed at the origin, and DFT is used to obtain the surrounding electron density. In CS the ion densities are also self-consistently obtained via a classical DFT equation identified to be a modified hypernetted chain equation (MHNC). Being all-electron models, the total electron density $n(r)$ includes bound and free states. In IS models, the surrounding ion distribution is assumed to vanish within the Wigner-Seitz cell and is not specified outside the cell. That is, other than the central nucleus, no other nuclei can be found in the range $r < a_i$. CS models use a large correlation sphere and include many field ions as well as a central nucleus within the CS. For a plasma at temperature $T > 0$, IS models begin with the grand potential, expressed as a functional of the electron density,

$$\Omega[n(r),T] = F_0[n(r),T] + F_{xc}[n(r),T] + \int d^3r\, n(r)\,(U[n(r)] - \mu_e)\,. \tag{8}$$

The first term in (8) represents the Helmholtz free energy of non-interacting electrons evaluated at the correct interacting density. The second term represents electron exchange and correlation (XC) contributions to the free energy. In the third term, $U[n(r)]$ is the Coulomb energy per particle, which includes the classical electrostatic energy of electrons with the central nucleus with charge $Z_{nuc}e$, and with each other (the Hartree term), *viz.*

$$U[n(r)] = -\frac{Z_{nuc}e^2}{r} + \frac{e^2}{2}\int d^3r'\,\frac{n(r')}{|\mathbf{r}-\mathbf{r}'|}. \tag{9}$$

The thermodynamic potential is stationary with respect to density-functional variations,

$$\frac{\delta\Omega[n(r),T]}{\delta n(r)} = 0 \tag{10}$$

This Euler equation gives the equilibrium electron density $n(r)$, and the grand potential $\Omega[n(r),T]$. The one-body potential associated with (9), which satisfies the usual Poisson equation, is obtained through this functional differentiation as

$$u[n(r)] = -\frac{Z_{nuc}e^2}{r} + e^2\int d^3r'\,\frac{n(r')}{|\mathbf{r}-\mathbf{r}'|}. \tag{11}$$

In some models, the electron chemical potential μ_e acts as a Lagrange multiplier for the conservation of electron number or, equivalently here, for overall charge neutrality, whereas in others it is specified and another variable acts as a Lagrange multiplier. We treat both cases in what follows.

Charge neutrality in IS models is used to specify zero electric field beyond a distance a_i, and the second boundary condition for the Poisson equation becomes

$$\frac{du}{dr} = 0, r \geq a_i. \tag{12}$$

This choice gives rise to a muffin-tin picture of potentials in the plasma. In a purely quantum mechanical scheme, boundary conditions must be associated with the orbitals - i.e., bound states decaying exponentially and the continuum states decaying to plane waves; the electrostatic boundary conditions are needed to ensure overall charge neutrality of the Z_{nuc} electrons in the IS.

DFT equations yield the radial density distribution $n(r)$ of the Z_{nuc} electrons within this charge-neutral fundamental cell. Result for the ion's effective charge, and

other information like the density of states of continuum electrons, can be calculated. The prototype of this class is the finite-temperature TF algorithm of Feynman, Metropolis, and Teller [56]. TF theory provides a basic comparison with improved ion-sphere models, and other improved models of dense plasmas. Below, we identify two MIS definitions within the context of TF theory. The introduction of orbitals and the addition of exchange and correlation interactions improve the standard TF description. Orbitals give rise to bound-state shell structure and continuum-state resonances, and exchange-correlation interactions bring in the many-body effects as an effective one-electron Kohn-Sham potential. Liberman's Inferno model [17], the non-relativistic Muze [51, 57] code used here, and the relativistic Purgatorio [58] and Paradisio (*sic*) [59] algorithms are all of this type, and they offer yet a third MIS definition.

The average atom model, and its different implementations in the codes mentioned in the previous paragraph, are all based on a spherical cell with one nucleus. A more general approach would contain both electron- and ion- equations, solved self-consistently, to yield electron and ion density distributions. This approach has been implemented previously by several authors within OFDFT [39–41] and in Kohn-Sham formulations [42]. The ion subsystem obeys classical statistical mechanics. Here, we employ an approach developed by Dharma-wardana and Perrot [20, 60–62].

In the correlation-function based DFT model of Dharma-wardana and Perrot [20, 60–62], one considers in principle the entire volume of the plasma surrounding the nucleus at the origin. Coupled DFT equations for the electron and ion densities $n_e(r)$ and $n_i(r)$ are solved out to some distance R_c (usually, $\sim 5-6$ times larger than the radius a_i), by when the correlations with the central nucleus have died off, and the densities of both species have approached asymptotic mean values. This R_c is the radius of a different fundamental cell, the CS, and we use that term to distinguish such two-component DFT models. The major improvement obtained are (i) the possibility of calculating electron bound states to cover the full extent of their exponential decay, (ii) continuum states to satisfy the Friedel sum rule, (iii) inclusion of the influence of neighboring ions on the electrons associated with a particular nucleus. The neighboring ions introduce features into the continuum density of states that result from multi-center scattering [63]; these can be important when Γ_{ii} is large, and Fig. 2 indicates that this is true for most of the temperature-density region of interest to us.

Dharma-wardana and Perrot [60] found that the local density approximation, which works well for electrons, was useless for treating the ion-ion correlations. They showed that the ion distribution was better determined by using the modified-hypernetted chain equations [10] to describe the non-local character of these interactions. It should be noted that the MHNC equation arises naturally in Re. [60] as a classical DFT equation, via a functional derivative of the free energy with respect to the ion-density. For many plasmas of interest it is found that the ion-ion pair correlation function can be replaced by a simple-cavity model, and this simplification is known as the neutral-pseudoatom (NPA) model [61]. In this approximation, the nucleus, the cavity, and the associated electron cloud form a nearly neutral object having many useful analytical properties. (The NPA model of Blancard and Faussurier [64] introduces a different treatment of ionic correlations.) In the NPA approach used here, where the average density of free electrons is specified as a boundary condition, one computes the average density of plasma ions (and, hence, the Wigner-Seitz radius). This is done self-consistently as the MIS is determined, by assuming that all plasma ions have this same net charge and that, in the asymptotic regime, the total charge density vanishes.

For the NPA, we construct three MIS definitions analogous to those of the orbital-based IS models. However, because of the different boundary conditions for the IS and CS models, two of the NPA definitions actually are the same, and the third yields a very similar MIS.

B. Electron Exchange and Correlation Interactions

The electron exchange-correlation potential, calculated as the functional derivative of the free energy $F_{xc}[n(r),T]$ with respect to the electron density $n(r)$ adds to the effective one-body potential $u[n(r)]$ of (11); this potential is given by:

$$\frac{\delta F_{xc}[n(r),T]}{\delta n(r)} \approx u_x[n,T]_r + u_c[n,T]_r, \qquad (13)$$

where we make the local-density approximation (LDA) in the final step, as indicated by the suffix $[...]_r$.. The separate exchange and correlation potential energies (per particle), $u_x[n,T]_r$ and $u_c[n,T_r]$, for homogeneous plasmas have been evaluated by Dharma-wardana et al., [67–69], Ichimaru et al., [72] and other workers [70, 71]. Conclusions from these include:

1. Limiting, low- and high-temperature expressions are well established for both $u_x[n,T]$ and $u_c[n,T]$. The exchange energy often has been approximated by a simple formula that interpolates between these limits [73]; thus,

$$u_x[n,T] \;=\; u_x[n,0]\left(1+\frac{3}{2\Theta[n]}\right)^{-1}, \qquad (14)$$

with the $T=0$ value $u_x[n,0] = -e^2(3n/\pi)^{1/3}$ being Dirac's original expression. However, a form which is essentially exact in all regimes, and correctly handles the logarithmic divergences in the zero-temperature limit is [68]:

$$u_x[n,T] \;=\; u_x[n,0]\tanh(1/t)\frac{N(t)}{D(t)}$$

$$N(t) = 1 + 2.8343t^2 - 0.2151t^3 + 5.2759t^4$$
$$D(t) = 1 + 3.9431t^2 + 7.9138t^4, \quad (15)$$

where $t = 1/\Theta[n]$. By comparison, the often used form (14) may be in error by as much as 50% in the warm dense matter (WDM) regime, $1 < \Theta < 10$. We also note that, in this regime, it is better to treat the exchange and correlation (XC) contributions together, because of strong cancellations that occur in their sum; this is consistent with a wide body of experience in developing and using zero-temperature functionals. Parametrization covering both exchange and correlation from $T = 0$ to finite-T are available from Ichimaru et al. [72], and from Perrot and Dharma-wardana [69]. The exchange potential given by (15) is the form that we will use here for ion-sphere models, although other forms have been used for average atoms models previously [57]. The correlation-sphere models reported here use the XC-parametrization of Perrot and Dharma-wardana [69].

2. At $T = 0$ the quantity $|u_c[n,0]/u_x[n,0]|$ does not exceed 0.3 for normal solid-state densities, and it is even smaller at higher densities. For $T < E_F$, exchange dominates over correlation, but a cross-over occurs around $\Theta = 1$, and as the plasma becomes hotter, exchange becomes unimportant.

3. At very low temperatures, $\Theta \gg 1$, $u_{xc}[n,T]$ is not a monotonic function of temperature. Also, the local degeneracy is high in high density regions near ion centers, and low in low-density regions at the edges of ion spheres. Therefore, accurate parameterizations covering all regimes, and including important cancellations between exchange effects and correlation terms should be used. That is, the combined quantity $u_{xc}[n,T]$ should be used.

4. At all densities the magnitude of $u_{xc}[n,T]$ (itself a negative quantity) decreases monotonically with temperature for $\Theta < 1/2$. *Thus, for studies of warm and hot dense matter, both exchange and correlation at finite-T are needed; and the zero-temperature quantity, $u_{xc}[n,0]$ is of uncertain validity at best.*

These stand in sharp contrast to those applicable to cold, compressed solids [74, 75], where $T = 0$ values are adequate. This conclusion is reinforced by Fig. 3, which is a surface map of $|u_{xc}[n,T]|$, from Perrot and Dharma-wardana [68] and used in the Muze and NPA calculations of this study. Curvature in the lines of constant $|u_{xc}[n,T]|$ highlight the temperature dependence of u_{xc}. Further, for the range of electron densities explored here ($10^{22} \le n_e \le 10^{25}$ cm^{-3}; $0.544 \le r_s \le 5.44$ a.u.), exchange-correlation interactions can reduce the chemical potential of plasma electrons by several eV, and reduce the MIS by a half unit or more (see Tables II-VII of Section IV).

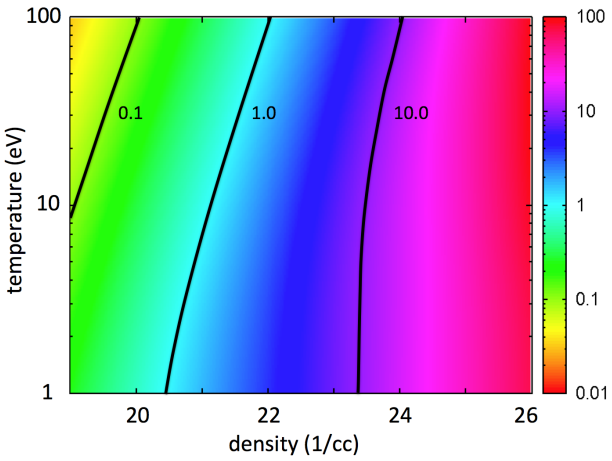

FIG. 3: (Color online) Surface map of the absolute magnitude of the finite-temperature exchange-correlation interaction of Ref. [68], in units of eV, for the homogeneous electron gas. Contour lines denote (from left) $|u_{xc}| = 0.1, 1.0, 10$ eV.

In section IV the consequences of the exchange-correlation contribution will be explored.

C. OFDFT and the Thomas-Fermi Model

In the Thomas-Fermi (TF) model [21, 55] two approximations are made to $\Omega[n(r),T]$: (i) The free energy of non-interacting electrons $F_0[n(r),T]$ is treated in the local density approximation (LDA), $F_0[n|_r,T]$, wherein electronic quantities for the inhomogeneous system are taken to be those of the homogeneous system at the local value of the density, viz., n= $n|_r$. (ii) In the original TF model, the XC-contribution to the kinetic energy, as well as to the potentials are neglected since $F_{xc}[n,T]$ is set to zero. The key advantage of the TF-model is that only an equation for the density needs to be solved. Such models are realizations of the original Hohenberg-Kohn-Mermin [18] formulation of DFT, rather than the Kohn-Sham approach discussed below.

The kinetic-energy contribution in TF models is:

$$F_0^{TF}[n,T] = \frac{\sqrt{2}e^2}{\pi a_0}\left(\frac{T}{e^2/a_0}\right)^{5/2} \cdot \int d^3r \left\{\xi[n] I_{1/2}(\xi[n]) - \frac{2}{3} I_{3/2}(\xi[n])\right\}, \quad (16)$$

where

$$I_\alpha(t) = \int dy \, \frac{y^\alpha}{1+\exp(y-t)} \quad (17)$$

is the Fermi-Dirac integral function and where

$$\xi[n(r)] = -\left\{U[n(r)] - \mu_e\right\}/T \quad (18)$$

The approximation (16) is accurate at high density. The Euler equation for this model leads to the usual finite-temperature TF result for the local density,

$$n(r) = \frac{\sqrt{2}a_0^3}{\pi^2}\left(\frac{T}{e^2/a_0}\right)^{3/2} I_{1/2}[\xi(r)]. \quad (19)$$

Once the above (non-linear) equations are solved and the chemical potential μ_e^{TF} determined through iteration, an MIS can be computed for the ion in the IS. The simplest prescription involves only the density at the sphere's edge where, because of boundary conditions, electrons experience no electrostatic forces:

$$\begin{aligned}\langle Z\rangle_{TF} &= \frac{4\pi a_i^3}{3} n(a_i) \\ &= \frac{4\sqrt{2}}{3\pi}\left(\frac{a_i}{a_0}\right)^3\left(\frac{T}{e^2/a_0}\right)^{3/2} I_{1/2}\left(\frac{\mu_e^{TF}}{T}\right) \quad (20)\end{aligned}$$

Feynman *et al.* [56] constructed the first hot, dense matter EOS using an electron pressure consistent with this estimate of the free electron density, and some modern EOS schemes [76] still do this. (Note, however, that the remaining thermodynamic quantities, such as the energy, are not constructed from the edge density.)

An alternative MIS definition for the TF model involves electrons that have, *locally*, negative total energy [40]. One first determines their density,

$$n_b^{TF}(r) = \frac{\sqrt{2}a_0^3}{\pi^2}\left(\frac{T}{e^2/a_0}\right)^{3/2} \cdot \int_0^{-U(r)/T} dy \frac{y^{1/2}}{1+\exp(y-\xi(r))}, \quad (21)$$

and then sums all such bound electrons within the ion sphere to obtain

$$Z_{TF}^* = Z_{nuc} - \int d^3r\, n_b^{TF}(r). \quad (22)$$

It is easy to see that $Z_{TF}^* > \langle Z\rangle_{TF}$ because not all of the enhanced density at small r-values represents electrons with negative total energy. This is illustrated in Fig. 4 for Al at normal solid density and 30 eV. Thus, counting these additional unbound electrons increases the MIS by about 20% (see Section IV for details).

Attention has been given to adding XC-interactions to the original finite-T TF scheme [55, 77]. It is worthwhile to note subtleties that arise when one considers the MIS definitions for TF calculations (TFxc) that include these terms. Our first Thomas-Fermi MIS definition, $\langle Z\rangle_{TF}$, uses the fact that Coulomb forces vanish at $r = a_i$, and hence that all electrons there are free. The quantity $u_{xc}[n(a_i), T]$, however, does not vanish at the edge of this sphere, but we reestablish the condition that all electrons at $r = a_i$ are free, *viz.* $n_b^{TFxc}(a_i) = 0$, by identifying this boundary value of u_{xc} as the exchange-correlation contribution u_{xc} to the chemical potential of the interacting electron gas outside the cell. Since $u_{xc} < 0$, it follows that $\langle Z\rangle_{TFxc} < \langle Z\rangle_{TF}$. Our second TF MIS definition, Z^*, identifies electrons with negative total energy, *viz.*,

$$n_b^{TFxc}(r) = \frac{\sqrt{2}a_0^3}{\pi^2}\left(\frac{T}{e^2/a_0}\right)^{3/2} \cdot \int_0^{-U'(r)/T} dy \frac{y^{1/2}}{1+\exp(y+u_{xc}(r)-\xi(r))}, \quad (23)$$

where now $-U'(r)/T = -(U(r)+u_{xc}(r))/T$. However, as defined in DFT, the exchange-correlation functional includes not only true potential energy terms arising from XC, but also the part of the kinetic energy neglected when the true free energy functional is replaced by a functional of non-interacting particles taken at the interacting density. Thus, in both definitions, we see an ambiguity arising from the fact that kinetic and potential energy contributions cannot be disentangled in the context of DFT.

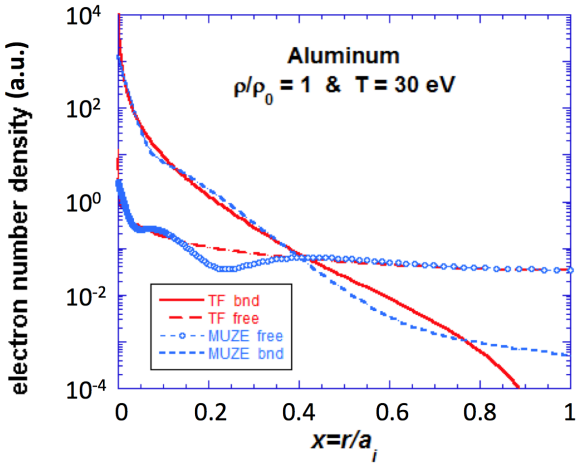

FIG. 4: (Color online) Behavior of bound (negative energy) and free (positive energy) electron densities, in atomic units, within an IS, for Al at normal solid density and $T = 30$ eV. There are fundamental differences between orbital-based and OFDFT models, here illustrated by Muze and TF calculations. In particular, with orbitals, bound electron density can extend beyond the sphere, and orthogonality of bound and continuum orbitals imposes obvious structure on the free electron density near the nucleus.

With regard to our MIS definition (22) for TF models, we see by the negative sign of $u_{xc}(n,T)$ at all r-values that it adds to the nuclear attraction; thus, the fraction of bound electrons is increased, leading to the result $Z_{TFxc}^* < Z_{TF}^*$, obtained by substituting (23) into (22). This conclusion is consistent with MIS calculations reported in Ref. [77], wherein an approximate, but different, T-dependent exchange interaction was used.

D. Orbital-Based DFT and the Muze Model

With XC interactions included in the TF model, further improvements result from adding gradient corrections to the non-interacting free energy $F_0[n,T]$. Such models, which attempt to retain $n(r)$ as the basic variable, fall in the category of orbital-free DFT [35–37]. New, more reliable forms for the kinetic energy as a functional of the electron density $n_e(r)$ have recently been developed [38]. Thus OFDFT methods have been over-shadowed by finite-temperature, orbital-based DFT models. Kohn and Sham [19] (KS), presented a solution to the kinetic-energy problem (extendable to finite-T as well) through the introduction of a special set of one-electron orbitals $\{\psi_s(r)\}$ that enables the non-interacting energy to be computed exactly if the exact XC free energy functional is known. These orbitals satisfy a one-body Schrödinger equation,

$$\left[-\frac{\hbar^2}{2m}\nabla^2 + U(r)\right]\psi_s(r) = \epsilon_s\psi_s(r). \tag{24}$$

The orbitals are constrained to be orthogonal via Lagrange multipliers which are the Kohn-Sham eigenvalues. The ground-state density of an N-electron system is constructed from the sum of the orbital densities $|\psi_s(r)|^2$ having the N lowest eigenvalues. This scheme exhibits shell structure that is missing in OFDFT models.

Mermin [78] extended the theory to nonzero temperatures. Here, bound-state solutions, with $\epsilon_s < 0$, again give rise to shells (although high plasma pressure severely limits the number of bound states), and continuum-state solutions $\epsilon_s \geq 0$ yield distorted plane waves. The eigenvalues ϵ_s, the Lagrange multipliers in the Kohn-Sham scheme, differ substantially from true eigen-energies. Similarly, the Kohn-Sham orbitals are not true electronic states. However, in most applications ϵ_s are used as energy eigenvalues, and $\psi_s(r)$ are used as one-electron orbitals without further discussion. The electron density $n(r)$ is constructed from a sum over the KS-orbitals and Fermi occupation probabilities

$$n(r) = \sum_s f(\epsilon_s,\mu_e)\,|\psi_s(r)|^2 \tag{25}$$

$$f(\epsilon,\mu) = (1+\exp[(\epsilon-\mu)/T])^{-1} \tag{26}$$

Mermin noted that, in the high density limit, the TF form of the electron density is regained.

In the present work, we use the code Muze [51, 57], which is an IS model, to explore the importance of both orbitals and XC-interactions for improving Thomas-Fermi estimates of MIS in ion-sphere models. For a specified nuclear charge, temperature, Wigner-Seitz radius, and choice of exchange-correlation interaction, Muze computes KS orbitals and eigenvalues from the non-relativistic, single-electron Schrödinger-like equation,

$$\left[-\frac{\hbar^2}{2m}\nabla^2 + U(r) + u_{xc}[n(r),T]\right]\psi_s(r) = \epsilon_s\psi_s(r). \tag{27}$$

The electron chemical potential μ_e^{Muze} is found by an iteration involving (25), from the requirement of overall charge neutrality for the ion sphere.

One benefit of an orbital-based DFT is its treatment of the largest portion of the kinetic energy operator. Relative to OFDFT formulations, this circumvents the need for approximate gradient corrections to the kinetic energy $F_0[n,T]$ that are often used to obtain reasonable cusps near the nuclei [21, 35–37, 55]; however, gradient corrections are still necessary in the exchange-correlation potential. Orbitals also lead to new physics not occurring in the TF model. Because Muze chooses boundary conditions in which the exponentially decaying tails of bound orbitals can extend beyond the IS radius, a portion of the density at $r = a_i$ (and beyond) actually represents electrons with negative energy, i.e., bound electrons not entirely confined to the IS. This phenomenon is illustrated in Fig. 4, which shows bound and continuum densities for Al at normal solid density and 30 eV. The contrasting behavior of (orbital-free) TF and (orbital-based) Muze densities is evident. For this reason, comparisons of the orbital-based MIS expression,

$$Z^{IS}_{Muze} = \frac{4\pi a_i^3}{3}n(a_i), \tag{28}$$

and the TF quantity $\langle Z\rangle_{TF}$ are of limited value because the density in (28) includes an unspecified contribution from bound (negative energy) electrons.

On the other hand, an analog of Z^*_{TF} can be obtained by summing the density of negative energy electrons within the ion sphere (Model A of Ref. [17]). Using only the few bound orbitals contained in the summation of (25), one identifies the bound electron density $n_b(r)$. hence we have:

$$Z^*_{Muze} = Z_{nuc} - \sum_{\epsilon_s<0}\left\{\omega(\epsilon_s)f(\epsilon_s,\mu_e)\int_{IS} d^3r\,|\psi_s(r)|^2\right\} \tag{29}$$

where now the sum is over energy states and ω is the degeneracy. Any bound electron density outside the ion sphere is excluded.

When a bound state is pressure ionized and moves into the continuum , the resulting resonance electrons close to the edge of the continuum retain much of their bound state character and contribute narrow peaks to the continuum density of states [35, 54, 58, 63]. Although a proper treatment of new resonances ensures that the plasma pressure varies smoothly [79–81], Z^* for orbital-based, ion-sphere models can undergo an abrupt, unphysical increase. Various ideas have been proposed to overcome this behavior [8], which is seen and discussed in Section IV.

As regards this second MIS definition, if, instead of a summation of bound-state orbital terms, an energy integration is performed with respect to the continuum KS-orbital terms in (25), $\{s \to \epsilon,\nu$, with ν representing any additional quantum numbers needed for specificity$\}$, one

can re-order integrations to obtain

$$Z^*_{Muze} = \int d^3r \left\{ \int_0^\infty d\epsilon f(\epsilon,\mu_e) \sum_\nu \omega_\nu \left|\psi_{\epsilon,\nu}(r)\right|^2 \right\} = \int d\epsilon f(\epsilon,\mu_e) \left[\int d^3r\, g(\epsilon,r) \right], \quad (30)$$

where $g(\epsilon, r)$ is an effective, local density of states (DOS) per unit volume. If we replace this effective DOS in (30) by $g_0(\epsilon)$, the DOS for an ideal gas,

$$g(\epsilon,r) \to g_0(\epsilon) = \frac{1}{2\pi^2}\left(\frac{2m}{\hbar^2}\right)^{3/2}\sqrt{\epsilon} \quad (31)$$

we obtain a MIS having the same form as $\langle Z\rangle_{TF}$ in the sense that the MIS is obtained from a Fermi-Dirac distribution with no interactions; however, this distribution involves the chemical potential of an orbital-based calculation in place of μ_e^{TF}, *viz.*

$$\langle Z\rangle_{Muze} = \frac{4\sqrt{2}}{3\pi}\left(\frac{a_i}{a_0}\right)^3 \left(\frac{T}{e^2/a_0}\right)^{3/2} I_{1/2}\left(\frac{\mu_e^{Muze}}{T}\right) \quad (32)$$

For orbital-based ion-sphere models, the difference $Z^* - \langle Z\rangle$ is an integral measure of non-ideal features in the computed DOS.

Once a Muze solution is found, one can construct the three MIS-values, $\left\{\langle Z\rangle_{Muze}, Z^*_{Muze}, Z^{IS}_{Muze}\right\}$, using, respectively, (32), (30), and (28).

E. Including Ion Correlations: Coupled-Densities Models

Here, we sketch the implementation of KS models that include ionic correlations beyond the IS, as developed by Dharma-wardana and Perrot [60]. Other, related models by Ofer et al. [39] and by Zakowicz et al. [40] employ orbital-free methods for the electron density and correlations within the ion density, but these will not discussed further here.

Our calculational scheme begins with a correlation sphere of radius $R_c \sim$ 5-8a_i, filled with a homogeneous electron fluid of specified temperature T and average electron density n_e; hence, the electron chemical potential is known. A charge-neutralizing ion fluid is also included. The choice of a correlation sphere radius R_c of $(5-8)a_i$ is chosen to be large enough to be greater than typical ion-ion correlation lengths for a given problem. Even at $R_c = 5a_i$ the cell is two orders of magnitude more voluminous than that of the IS-model. Electron correlations die much faster than ion-correlations and are easily contained in the CS. A nucleus of charge $Z_{nuc}e$ is placed at the origin in the fluid, pulling electrons around it and causing a local modification $\Delta n_f(r)$ of the free electron density in the CS; bound states may form, causing an additional local enhancement $n_b(r)$. Thus the nucleus acquires some mean ionization Z due to population of bound states and free states. This Z is taken as a trial value for the effective charge of "field ions", whose mean number density becomes $n_i = n_e/Z$. In effect, in this algorithm Z is the Lagrange multiplier that enforces charge neutrality. This interpretation of MIS was first discussed in Ref. [60] in the context of hydrogen plasmas. The field ions are allowed to interact with other charges and form a correlated equilibrium distribution about the central nucleus. The coupled Euler equations for the electron and ion subsystems arise from the stationary property of the total free energy $F[n_e(r), n_i(r)]$ with respect to functional derivatives of the two densities. The electron-subsystem Euler equation $\delta F/\delta n_e(r) = 0$ leads to a Kohn-Sham like equation, while the ion-subsystem Euler equation, $\delta F/\delta n_i(r) = 0$ leads to an MHNC equation. The equations are coupled through the Lagrange multiplier Z, and via electrostatic and correlation potentials. Iterative solution of the coupled equations lead to the thermodynamic $n_e(r)$ and $n_i(r)$ profiles. The charge density profiles established around Z_{nuc} are

$$q_e(r) \equiv -en_e g_{ei}(r) = -e\left[n_e + \Delta n_f(r) + n_b(r)\right] \quad (33)$$

$$q_i(r) \equiv Z_{nuc}e\delta(r) + Zen_i g_{ii}(r) = Z_{nuc}e\delta(r) + Ze\left[\Delta n_i(r) + n_i\right], \quad (34)$$

where $g_{ei}(r)$ and $g_{ii}(r)$ are the electron-ion and ion-ion pair distribution functions, and where $\Delta n_i(r)$ represents the modification of the ion density from the bulk value. The calculation also yields the chemical potential of the ions.

The computation is begins with trial electron and ion density profiles. The value of Z, as well as the associated Wigner-Seitz radius b_i which is the trial value of a_i, are adjusted at each iteration using the calculated $n_b(r)$ and $\Delta n_f(r)$, while $\{R_c, T, n_e\}$ are held fixed. Solutions to the coupled DFT equations for the densities are iterated until, at $r = R_c$ and beyond, they yield a stationary value for the ratio $n_e/n_i = Z$, which we take to be the definition of the mean ionization $\langle Z\rangle$. The chosen CS is deemed large enough if both pair distribution functions have tended to unity, and if all bound-state orbitals have decayed exponentially while the continuum solutions have become phase-shifted free-electron orbitals. Consistency requires that at R_c the phase shifts of the continuum orbitals satisfy the Friedel sum rule, adding up to the value of the mean ionization $\langle Z\rangle$.

F. The Neutral Pseudo-Atom (NPA) Model

The above coupled-densities model, which has been implemented in several investigations, provides a systematic method with only a minimum of assumptions. However, a simpler version, when applicable, enables one to decouple the KS (electron) calculation from the ion profile calculation, so that the electron density can be addressed separately [20, 60–62], using a very simple model for the

ion profile. This simplification is based on the concept of the "neutral pseudoatom" (NPA), i.e., a single nucleus and *an associated cavity* embedded in a responsive electron gas with a compensating, uniform ionic background of charge density q_i. Properties of the NPA model are such that, to a good approximation, the total density of electrons in the plasma is the superposition of the pseudoatom densities surrounding individual ions.

To construct a neutral pseudoatom, a spherical cavity of radius b_i is made in the positive ion background; an amount of charge $\Delta Z = 4\pi b_i^3 q_i/3$ is thereby scooped out. A nucleus Z_{nuc} is placed at the cavity's center, and an inhomogeneous electron charge density $q_e(r) = -en(r)$, determined from KS orbitals, is established in response to this nucleus and the static, positive background with its spherical cavity. Effectively, the true ion-ion pair distribution function has been replaced by an approximation,

$$g_{ii}(r) = \theta(r - b_i), \tag{35}$$

where $\theta(x)$ is the usual step function. This cavity plus its contents is similar to the Wigner-Seitz sphere used in ion-sphere models; however, we emphasize that the charge density $q_e(r)$ belongs not only to the central nucleus, but also to the charge inhomogeneity associated with the cavity. However, this is a small perturbative effect compared to that of the central nucleus. Hence, as detailed by Perrot [89], linear response theory can be used to correct for the presence of the cavity, since the cavity potential induces a density displacement. Thus the electron density attributable to the NPA is given by

$$q_e(r) = -e\left[n_e + \Delta n_f(r) - \Delta n_f^{cavity}(r) + n_b(r)\right], \tag{36}$$

with free- and bound-state contributions analogous to the terms in (33). The NPA calculation uses the CS so its boundary conditions ($r = R_c$) for KS orbitals are the same as those applied to the full coupled-densities model. With a self-consistent NPA electron density in hand, the free-electron excess $\Delta\tilde{N}_f(r) = \Delta n_f(r) - \Delta n_f^{cavity}(r)$ can be used to determine a pair potential for evaluating the ion-ion $g_{ii}(r)$ obtained from a modified HNC equation, but this feature of the NPA model is not needed when its MIS-value is determined.

The KS orbital equation for the electrons, (27), must be solved iteratively for each orbital, with the cavity radius b_i being adjusted so that at each step $4\pi b_i^3 n_e/3 = Z$, where the effective charge Z is that of the nucleus Z_{nuc} minus the part of all its bound electrons that can be attributed to a single ion. When any of the bound states extend beyond the cavity, it is necessary to construct a method of sharing these delocalized, or "hopping" electrons so that only a suitable fraction of them are attributed the central nucleus. To this end, Perrot [61] introduced a cutting function $f(r)$ that applies to the delocalized states. This function, which integrates to unity, was constructed by studying results from full, two-component DFT calculations, and with it one expresses the effective number of bound electrons as

$$\nu_b = \int_{CS} d^3r f(r) n_b(r), \tag{37}$$

where the integration is over the volume of the CS (effectively, all space, since all bound states have decayed exponentially by $r = R_c$). Similarly, the number of electrons that contributes to a quasi-bound mobility edge, as in disordered semiconductors, can be written as

$$\nu_h = \int_{CS} d^3r \left[1 - f(r)\right] n_b(r). \tag{38}$$

These electrons cannot be assigned to any one ion center. When the number of quasi-bound electrons is substantial, say, $\nu_h > 1$, then the coupled electron/ion DFT equations should be used instead of their approximate, NPA version. Note that only a part of the total bound electrons n_b is included in ν_b, since the hopping electrons are not ascribed to any ion center, but belongs to the ion distribution. The theory of hopping electrons in plasmas has been discussed by Dharma-wardana and Perrot [62].

Equations for the NPA are iterated until self-consistency is obtained. At that point, the quantity

$$\langle Z \rangle_{NPA} = Z_{nuc} - \nu_b. \tag{39}$$

is identified as the MIS of the neutral pseudo-atom, and b_i converges to a_i, the computed radius of the Wigner-Seitz sphere for the central ion.

We may compare the correlation-sphere approach with the ion-sphere model MIS-value of $\langle Z \rangle$ by noting that the MIS sets the ratio of uniform electron and ion densities at the edge of the CS, i.e., $\langle Z \rangle_{NPA} = n(R_c)/n_i$, while the ion-sphere model uses the values at the edge of the ion-sphere, as in Eq. 28.

All the models, including the NPA, examined in this paper are "average-atom" models. There is just one species of field ions, with the MIS charge Z. The resulting $\langle Z \rangle_{NPA}$ need not be an integer. A simple extension of the average atom model is to consider the plasma to consist of several stages of ionization Z_i with composition fractions x_i. Here Z_i are integers, as in an Al-plasma with $Z_1 = 3$, $Z_2 = 2$ and $Z_3 = 3$ with an average atom value which is a non-integral quantity between 1 and 3. Then the average-atom mean ionization is usually found to be a simple approximant to the multi-species estimate of the mean ionization given by

$$\langle Z \rangle = \sum_i x_i Z_i \tag{40}$$

In the multi-species DFT calculations [8] using the NPA model or CS model, the equation of state is also computed, and the composition fractions are determined by a minimization of the total free energy as a function of x_i. Thus an aluminum plasma at a compression of 0.507 (i.e., about half the normal density), and at $T = 1.5$ eV is found to have a mean ionization state of $\langle Z \rangle$=1.478.

This fractional mean value is found to correspond to a multi-species plasma of Al^{1+}, Al^{2+}, and Al^{3+} with composition fractions 0.614, 0.294, 0.092. These numbers are obtained from the multi-species extension of the NPA model as described in [8]. The three types of ions and electrons provide a 4-component plasma (i=e,Al^{1+}, Al^{2+}, and Al^{3+}) with 10 different pair distribution functions (PDFs) $g_{ij}(r)$ that were determined via a set of coupled MHNC equations and the Kohn-Sham equations. This is a highly degenerate system which can be treated by AIMD methods. However, to date AIMD results are not available to test these calculations and the PDFs, electrical conductivities etc., predicted by [8]. Judging by previous experience, we are confident that when such results become available, good agreement with AIMD would be found.

The results from the average-atom models, and from the full multi-species approaches agree unless the plasma is close to ionization thresholds and phase-transitions. The multi-species DFT model establishes the thermodynamic character of $\langle Z \rangle$, already familiar from the simplest ionization models of Saha theory where particle interactions are ignored.

IV. MEAN IONIZATION STATE CALCULATIONS FOR BE, AL, AND CU

We now present and discuss mean ionization results for the different models described in Section III. It is helpful, first, to collect the equations used for the MIS definitions in various models, and this we do in Table I. With regard to recent, related work of Sterne et al. [80] using Purgatorio, the notational connections are: their $Z_{WS} \leftrightarrow Z^{IS}_{Muze}$, their $Z_{background} \leftrightarrow \langle Z \rangle_{Muze}$ and their $Z_{continuum} \leftrightarrow Z^{*}_{Muze}$. Notation in *most* of the cited NPA papers of Perrot and Dharma-wardana is such that their $\overline{Z} \leftrightarrow \langle Z \rangle_{NPA}$.

TABLE I: Equations for MIS calculations in different models.

model:	TF	Muze	NPA
cell :	IS	IS	CS
$\langle Z \rangle$	(20)	(32)	(39)
Z^*	(22)	(30)	...

We studied the metals Be, Al, and Cu under temperature and density conditions of contemporary laboratory interest. Tables II through VII list results computed for a representative set of points in the WDM regime, where the range of the electron degeneracy parameter $\eta_e = \mu_e/T$ is $\pm$ few. Material densities are expressed as compressions relative to normal solid density. (Again, for Be, Al, and Cu, respectively, $\rho_0 = 1.85, 2.70$, and 8.92 g/cm^3.) For each table, the ion density n_i, the Wigner-Seitz radius a_i, and the ion-ion coupling factor (computed using $\langle Z \rangle_{NPA}$) are listed. Column headings identify the particular model, and whether the calculation includes exchange-correlation interactions (as given in (15)). Entries are the electron chemical potential μ_e, and the MIS values $\langle Z \rangle$ and Z^*. Given the statements in Section II, we pay particular attention here to differences in μ_e-values obtained from the different models. In each table, reading from left to right reveals the effects of going beyond basic TF to include: (1) orbitals; (2) orbitals plus exchange-correlation; and, lastly, (3) orbitals, exchange-correlation, and a larger fundamental cell.

TABLE II: Mean ionization of Be: $\rho/\rho_0 = 1.0$ and $T = 10$ eV.

$n_i = 1.24 \cdot 10^{23}$ cm^{-3}, $a_i/a_0 = 2.32$, $\Gamma^{NPA}_{ii} = 4.63$				
DFT model:	TF	Muze	Muze	NPA
xc:	no	no	yes	yes
μ_e (eV)	5.06	4.72	3.39	7.77
$\langle Z \rangle$	1.73	1.69	1.53	2.00
Z^*	2.17	2.00	2.00	...

TABLE III: Mean ionization of Al: $\rho/\rho_0 = 0.1$ and $T = 10$ eV.

$n_i = 6.03 \cdot 10^{21}$ cm^{-3}, $a_i/a_0 = 6.44$, $\Gamma^{NPA}_{ii} = 2.14$				
DFT model:	TF	Muze	Muze	NPA
xc:	no	no	yes	yes
μ_e (eV)	-25.0	-26.2	-27.5	-26.2
$\langle Z \rangle$	2.53	2.26	1.98	2.25
Z^*	3.01	2.52	2.27	...

TABLE IV: Mean ionization of Al: $\rho/\rho_0 = 1.0$ and $T = 10$ eV.

$n_i = 6.03 \cdot 10^{22}$ cm^{-3}, $a_i/a_0 = 2.99$, $\Gamma^{NPA}_{ii} = 8.30$				
DFT model:	TF	Muze	Muze	NPA
xc:	no	no	yes	yes
μ_e (eV)	2.61	1.10	-0.77	2.76
$\langle Z \rangle$	2.96	2.64	2.28	3.02
Z^*	4.00	3.11	3.02	...

Along the model sequence TF $\rightarrow$ Muze (no xc) $\rightarrow$ Muze (recall that this an IS model), one can see that each of the three tabulated quantities decreases monotonically as first orbitals and then orbitals with exchange-correlation interactions are introduced. Values of $\langle Z \rangle$ will be close when electron degeneracy parameters computed by a pair of models are about the same and, for small differences, properties of the Fermi-Dirac integrals yield the relation $\Delta \langle Z \rangle \approx (\Delta\eta_e/2)\, I_{-1/2}(\eta_e)$. If one considers only the values of $\langle Z \rangle$, the effects of orbitals and exchange-correlation interactions tend to be comparable; on the other hand,

TABLE V: Mean ionization of Al: $\rho/\rho_0 = 1.0$ and $T = 30$ eV.

$n_i = 6.03 \cdot 10^{22}$ cm^{-3}, $a_i/a_0 = 2.99$, $\Gamma_{ii}^{NPA} = 5.60$				
DFT model:	TF	Muze	Muze	NPA
xc:	no	no	yes	yes
μ_e (eV)	-37.7	-40.5	-44.9	-37.4
$\langle Z \rangle$	4.26	3.93	3.42	4.30
Z^*	5.18	4.78	4.16	...

TABLE VI: Mean ionization of Al: $\rho/\rho_0 = 10.0$ and $T = 30$ eV.

$n_i = 6.03 \cdot 10^{23}$ cm^{-3}, $a_i/a_0 = 1.39$, $\Gamma_{ii}^{NPA} = 9.44$				
DFT model:	TF	Muze	Muze	NPA
xc:	no	no	yes	yes
μ_e (eV)	72.0	67.0	60.6	48.9
$\langle Z \rangle$	5.67	5.25	4.70	3.80
Z^*	7.40	4.50	3.81	...

if one considers instead only the Z^*-values, in all cases orbitals have the larger effect. It is the latter result that is consistent with expectations raised in Section III.

It is reassuring that, since the same exchange-correlation interaction energy is used, the values of Z^*_{Muze} and $\langle Z \rangle_{NPA}$ usually are very close. In light of comments made above, this means that ν_h is very small and that the NPA model is a good approximation of the full, two-component DFT model. But, it is disconcerting that often there are large differences between the corresponding electron chemical potentials. There is, however, a straightforward explanation that we mentioned earlier: In the NPA model and as required by KS theory [19, 21], the chemical potential is the non-interacting value at the interacting, homogeneous electron density which prevails in the bulk of the plasma. That is, μ_e is fixed by the electron density $n(R_c)$ specified at the edge of the correlation sphere. However, for orbital-based ion-sphere models such as Muze, the density at which μ_e is established is actually not that of a homogeneous, interacting electron gas: The central ion's influence usually is still felt at the boundary, $r = a_i$, as evidenced by KS orbitals not yet having attained their asymptotic values. Interestingly, this problem does not arise in the orbital-free, TF model since, at $r = a_i$, there are no electrons with negative total energy and there is no residual influence of the central ion on electrons with positive total energy.

Figures 5 through 8 reveal additional MIS trends and information. In Figs. 5, 6, and 7 we show computed values of MIS and η_e for a wide range of temperatures, for each of the metals Be, Al and Cu at normal solid density. For Be and Al, the temperature dependence of MIS-values shown in Figs. 5 and 6 is smooth, and the results for NPA and Muze tend to lie somewhat lower than those for TF and Muze-noxc. Here again we see the

TABLE VII: Mean ionization of Cu: $\rho/\rho_0 = 1.0$ and $T = 30$ eV.

$n_i = 8.41 \cdot 10^{22}$ cm^{-3}, $a_i/a_0 = 2.67$, $\Gamma_{ii}^{NPA} = 15.3$				
DFT model:	TF	Muze	Muze	NPA
xc:	no	no	yes	yes
μ_e (eV)	-13.8	-16.2	-21.8	-13.6
$\langle Z \rangle$	6.18	5.79	4.93	6.72
Z^*	8.08	6.74	5.79	...

expected effect on the MIS as first orbitals and then orbitals plus exchange-correlation interactions are added to the ion-sphere model. The exception is Cu, where Fig. 7 shows that Z^*_{Muze} drops abruptly by several charge states from a value of 11 at temperatures near 10 eV. This anomalous and unphysical behavior is due to the way this MIS apportions states that are continuum resonances at low temperature but evolve to bound, $3d$ orbitals as the temperature and, hence, the core charge increases. The abrupt change is not evident in Muze values of $\langle Z \rangle$ or in the corresponding values of η_e, both of which vary smoothly. In the right/lower panels of Figs. 5, 6, 7 the common trend of smaller differences in η_e, between Muze and NPA, as the temperature rises, confirms the increased reliability of ion-sphere models as electron degeneracy, Coulomb coupling, and exchange-correlation effects all decrease.

Figure 8 highlights the effects of pressure ionization, in plots of mean ionization (Muze) versus density for Al and Cu at $T = 30$ eV. The trend in Z^* is, first, one of decreasing ionization with increasing density, interrupted by small jumps when outer orbitals become pressure ionized. Later, large jumps occur in the region of increasing ionization when core orbitals are pressure ionized. As above, $\langle Z \rangle$ follows the general trend of Z^*, but without near discontinuities. Here, three points are noteworthy: (1) This behavior of first decreasing and then increasing ionization vs. density occurs over a modest range of plasma temperatures, as shown qualitatively by the TF values of $\langle Z \rangle$ for Al (at $20 \leq T \leq 40$ eV) that are plotted in Fig. 1. (2) In ion-sphere models, large MIS differences $|Z^* - \langle Z \rangle|$ signify important resonant structure in the continuum DOS. (3) Quite similar, nearly discontinuous ionization behavior has recently been published for gold and aluminum at low temperatures, $T \leq 10$ eV, using the NPA model [9]. Evidently, the pressure ionization jumps shown in Figs. 7 and 8 are a possible feature of all orbital-based average-atom models.

Figure 9 shows the run of the different MIS values computed by Muze (exchange-correlation included) versus temperature for Al at normal solid density. As the temperature drops, we see a growing difference between $\langle Z \rangle$ and the third MIS quantity, Z^{IS}_{Muze} (28). Because that difference is a measure of bound electron density at $r = a_i$, we have yet another indication that an ion sphere is not a large enough fundamental cell for determining

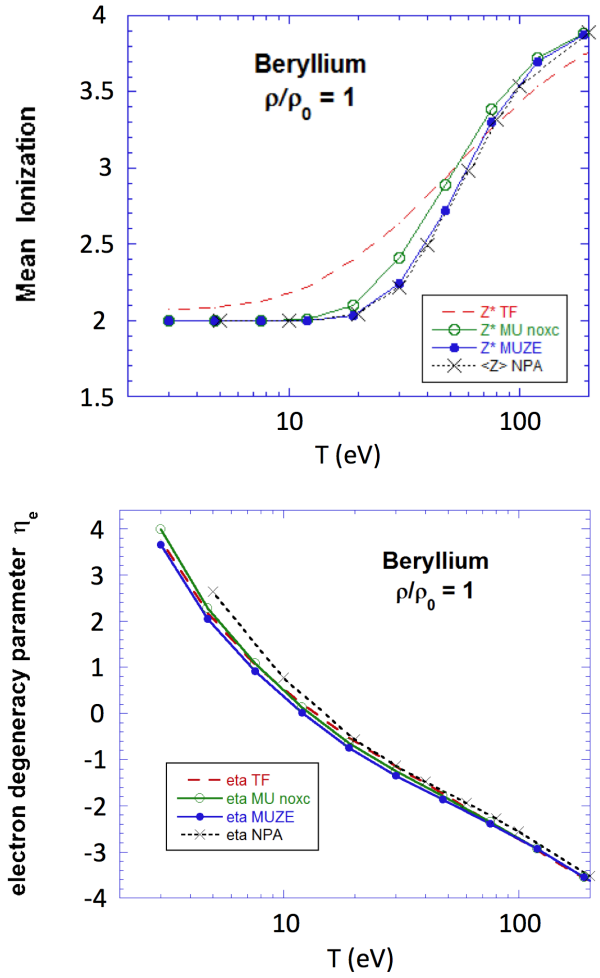

FIG. 5: (Color online) Plots of mean ionization (top panel) and electron degeneracy η_e (bottom panel) for Be at normal solid density, versus temperature, as determined by DFT models discussed in the text: Thomas-Fermi [TF], Muze without exchange-correlation [MU noxc], Muze with exchange-correlation [Muze], and neutral pseudo-atom [NPA].

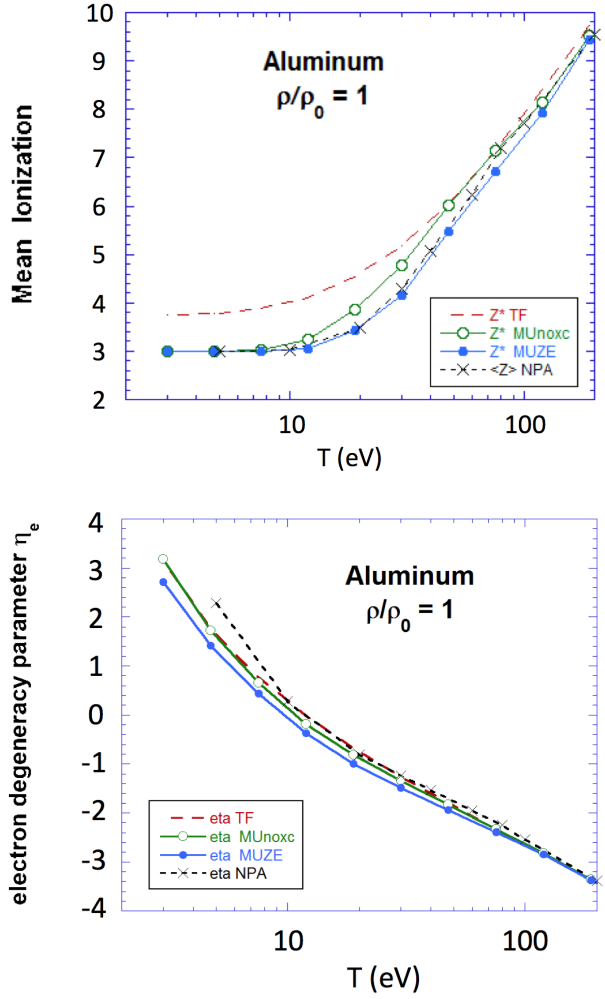

FIG. 6: (Color online) As in Fig. 5, for Al at normal solid density.

certain properties of strongly coupled systems. Figure 9 (right/lower panel) shows the run of $\langle Z\rangle$ versus temperature, as determined by the three ion-sphere models, for Cu at normal solid density. For comparison, we also plot NPA results. These curves illustrate the sensitivity of this MIS to the computed differences in electron chemical potentials.

To illustrate MIS sensitivity to the exchange-correlation potential, in Fig. 10 we plot $\langle Z\rangle$-values for Al, as calculated by Muze with different forms of $u_{xc}[n,T]$, for two temperatures and a range of densities. At $T = 1$ eV, $\langle Z\rangle$ is practically independent of the temperature or the exact form of u_{xc}, confirming the recent AIMD results of Faussurier et al. [82]. However, at $T = 30$ eV, the two temperature-dependent formulations of the exchange-correlation interaction both lead to a lower $\langle Z\rangle$ than that corresponding to the $T = 0$ potential that was used in, for example, Ref. [58]; also, values with the Iyetomi & Ichimaru formulation [72] lie closer to the $T = 0$ result than do those with the formulation by Perrot and Dharma-wardana (used in the other calculations reported herein) [71]. We also note the interesting result that $\langle Z\rangle$ here decreases with temperature at above-solid densities.

We conclude this section with some comments on the TF model. In general, TF results for (isolated) neutral atoms (at $T = 0$) are expected to be better for heavier elements, because a greater fraction of the electrons have large principal quantum numbers and so are less localized; hence, the uniform density approximation of $F_0[n,T]$ is more accurate. For cool-to-warm (say, $T \leq 10$ eV) dense matter, data plotted in Figs. 5-7 suggest a more complicated trend: The TF values of Z^* are reasonably close to those of the orbital-based DFT models for Be, but the relative agreement worsens as the nuclear charge Z_{nuc} increases. As Fig. 3 illustrated, exchange-correlation interactions are more important at low tem-

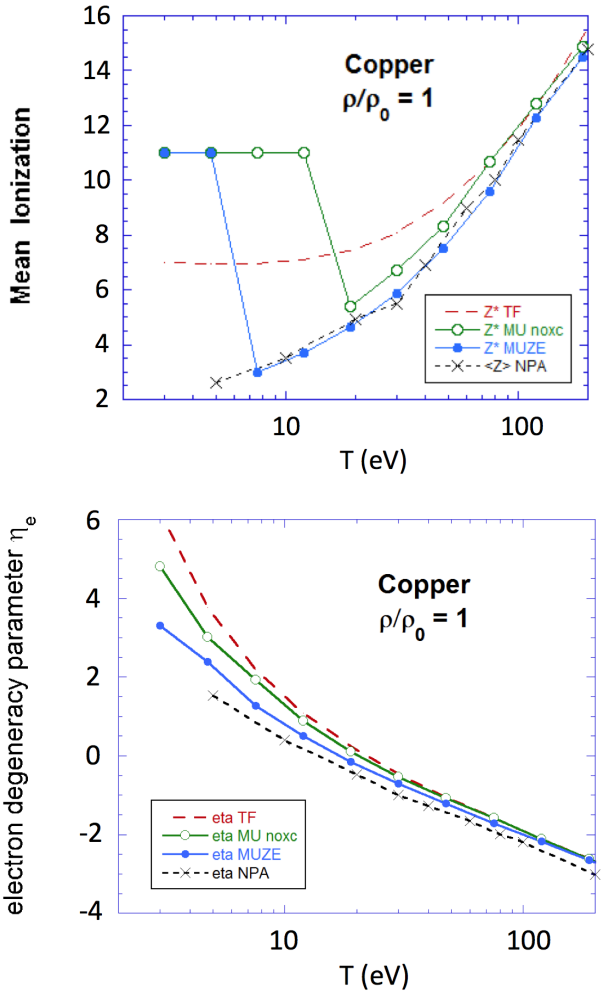

FIG. 7: (Color online) As in Fig. 5, for Cu at normal solid density.

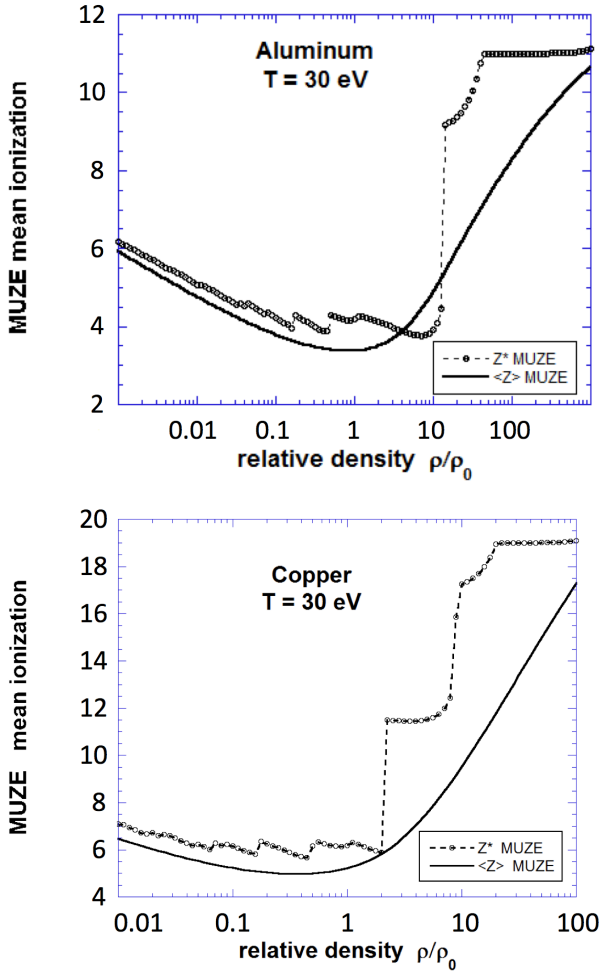

FIG. 8: (Color online) Mean ionization values Z^* and $\langle Z\rangle$, as calculated by Muze, for Al (top panel) and Cu (bottom panel) at $T = 30$ eV, versus density. See text for discussion of abrupt jumps in Z^*.

peratures. However, by comparing the Z^*-values plotted here for all three ion-sphere models, we see that in fact orbitals have a relatively greater effect at low temperatures while exchange-correlation interactions have relatively greater effect than orbitals at high temperatures. Such results suggest caution when applying "conventional wisdom" to plasmas having partial ionization and partial degeneracy! There also is a trend, most apparent in Fig. 5, where TF theory overestimates the more accurate values of Z^* for low ionization, but underestimates them for high ionization. Finally, the tabulated results that $\langle Z\rangle_{TF}$ (the simplest MIS calculation) sometimes turns out to be close to Z^*_{Muze} and $\langle Z\rangle_{NPA}$. This situation results from a partial cancellation of two effects: (1) the enhanced density of continuum electrons counted in Z^*_{Muze} and $\langle Z\rangle_{NPA}$ and (2) the enhanced binding due to exchange-correlation effects. Unfortunately, (cf. Table IV and Fig. 8), such fortuitous agreement disappears at the densities of compressed solids, where pressure ionization of orbitals is significant.

V. X-RAY THOMSON SCATTERING AS A PROBE OF MEAN IONIZATION

X-ray Thomson scattering (XRTS) is an important diagnostic for a variety of hard and soft condensed matter systems. XRTS also has the promise to provide useful information about dense plasmas that cannot be obtained otherwise [83], due to their short existence. MIS concepts are central to understanding dense-plasma XRTS, and here we consider these experiments in the context context of MIS.

A popular formulation of XRTS by electrons in plasmas and liquid metals is due to Chihara [84], where the XRTS cross section per nucleus, differential in frequency and direction of scattered radiation, is

$$\frac{d^2\sigma}{d\Omega_f d\omega} = \frac{d\sigma_{Th}}{d\Omega_f}\frac{k_f}{k_i}S^{tot}_{ee}(k,\omega), \tag{41}$$

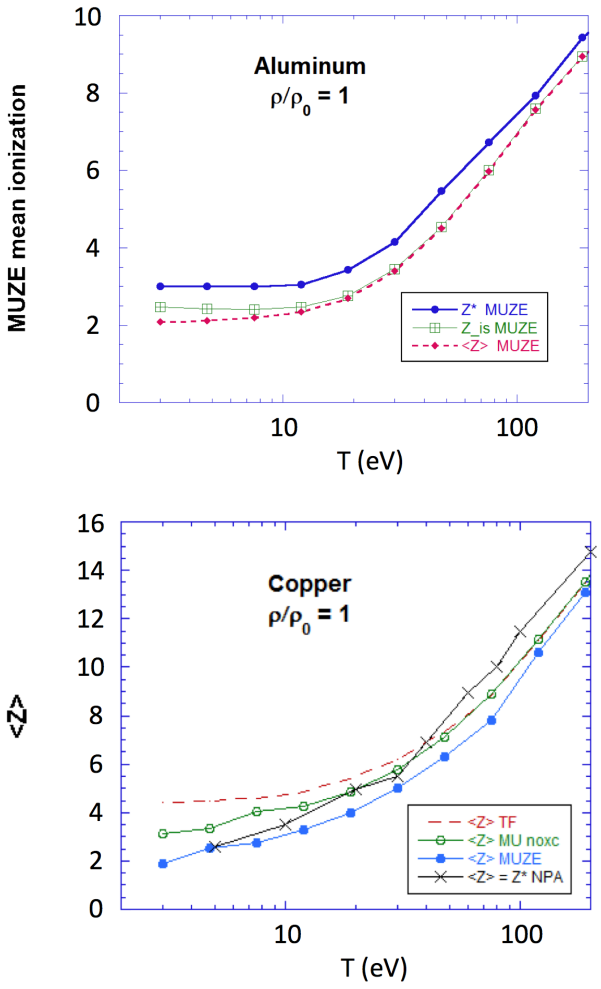

FIG. 9: (Color online) (top) Comparison of the three different MIS values defined in the Muze model ((20), (28), and (32)), for Al at normal solid density, versus temperature. (bottom) Comparison of $\langle Z\rangle$-values for Cu at normal solid density, as computed by different DFT models ((20), (32), and (39)), versus temperature.

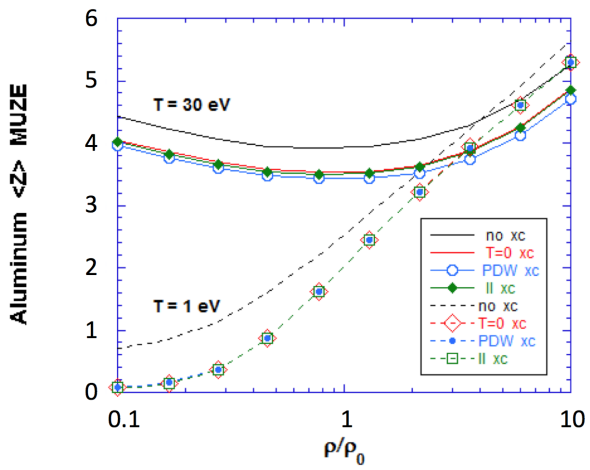

FIG. 10: (Color online) The density dependence of Al $\langle Z\rangle$ calculated by Muze, at two temperatures and with four different treatments of the exchange-correlation potential (including no xc). PDW denotes Ref. [69] and II denotes [72].

Here $\hbar\omega$ and $\hbar k$ are the energy and momentum lost when a photon of incident wavevector $\mathbf{k}_i$ (as modified by the plasma's index of refraction) is scattered into the solid-angle element surrounding the final wavevector $\mathbf{k}_f$, and where $d\sigma_{Th}/d\Omega_f$ is the usual differential Thomson cross section for scattering of unpolarized radiation by electrons. All effects of the medium are contained in the electrons' total dynamic structure factor, $S_{ee}^{tot}(k,\omega)$, which includes contributions from both bound and free electrons, as well as ionic contributions to the electron dynamics.

Chihara's analysis assumes the separability of an ion's electrons into: (1) core electrons Z_c that are tightly bound, and hence highly localized; and (2) so-called free electrons, that are delocalized. This latter group includes all electrons having positive energy, plus valence electrons that are only weakly bound. These are $Z_f = Z_{nuc} - Z_c$ per ion, where, as before, Z_{nuc} is the nuclear charge. Similarly, their densities sum to give the total electron density associated with that nucleus, $n(r) = n_c(r) + n_f(r)$. Thus we see that superpositions and overlaps of electron densities are not adequately treated. Chihara's principal result is that the dynamic structure factor appearing in (41) has three contributions, commonly written as:

$$S_{ee}^{tot}(k,\omega) = |n_f(k) + n_c(k)|^2 S_{ii}(k,\omega) + Z_f S_{ee}^{(0)}(k,\omega) + Z_c \int d\omega' S_{ce}(\omega-\omega') S_s(k,\omega'). \quad (42)$$

The first term on the rhs is a product involving the usual ion-ion dynamic structure factor and the Fourier transform of $n(r)$. This term represents low-frequency, inelastic scattering by electrons that follow the ion motion [48]; it is often referred to as the "quasielastic peak". The second term contains the structure factor $S_{ee}^{(0)}(k,\omega)$ that represents high-frequency electron dynamics that are not correlated with ion motion. The third term involves a convolution of special dynamic structure factors pertaining to the core electrons and to a gas of non-interacting ions, and it represents inelastic scattering by the electrons tightly bound to ions; details of the notation can be found elsewhere [84]. Our interest is with the quantities multiplying each of these structure factors.

The essential problem is that in dense plasmas the electron separation $n_c(r)+n_f(r)$ that Chihara posits is a delicate matter which depends on the nature of the probe and the material itself. In simple metals and their plasmas, there is a clear energy separation between valence electrons from core electrons. The same feature also exists in weakly-coupled plasmas in which isolated-atom electronic structure calculations can be used to designate deeply bound or completely free electrons (such models are used in the "chemical picture", and in Saha-like ion-

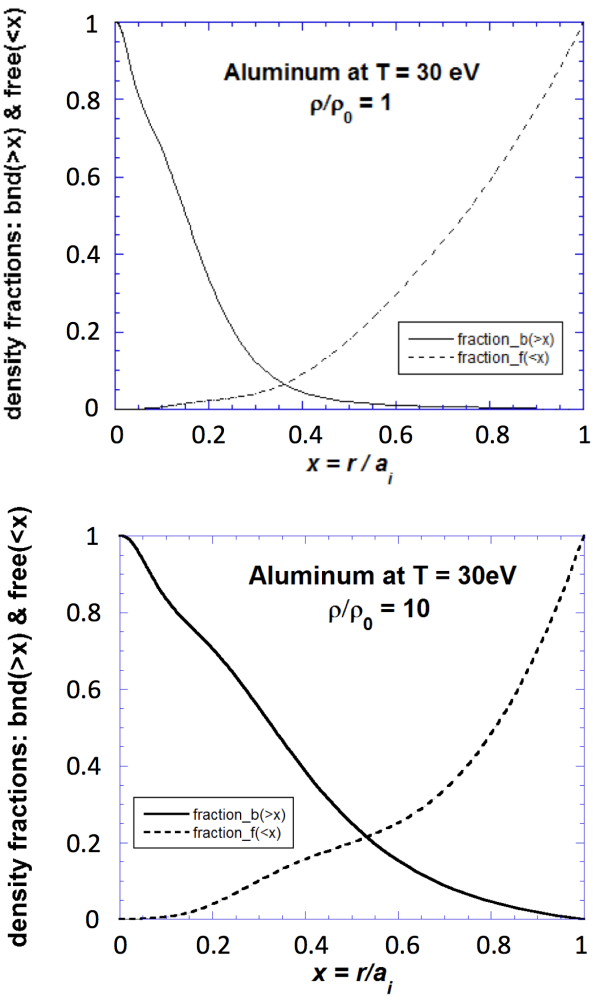

FIG. 11: The integrated fraction of bound ($\epsilon < 0$) electron density *outside* the radius $r = xa_i$, and the integrated fraction of free ($\epsilon \geq 0$) electron density *inside* the radius $r = xa_i$, as computed by Muze. (top) Al at $T = 30$ eV and $\rho/\rho_0 = 1$, with other details listed in Table IV. (bottom) Al at $T = 30$ eV and $\rho/\rho_0 = 10$, with other details listed in Table IV.

ization equations for weakly coupled systems). However, in most plasmas the electronic structure of ions has to be calculated using some model like the ones described here. The separation between "core" and free electrons must be carried out, paying attention to the overlap of bound-electron distributions between ions. Nor is there a separation in configuration space (a measure of localization; recall (25)) and, hence, in k-space forced by the orthogonality of KS orbitals. This is evident in Fig. 4, which plots bound (i.e., negative energy) and free (i.e., positive energy) electron densities versus position r, for solid-density Al at 30 eV. Clearly, the bound electrons are only slightly localized relative to the free electrons. Another way of displaying the information in Fig. 4 is shown in Fig. 11, where integrated Al densities - total bound density within r and total unbound density beyond r - are plotted. The left panel is, again, for solid density Al at 30 eV; the right panel is for Al at the same temperature but the higher density, $\rho/\rho_0 = 10$. We see that greater compression leads to greater delocalization of negative energy states and to greater uncertainty in any assignment of core vs. free, in these regimes of compression and temperature.

These issues complicate the use of distinct XRTS features to determine MIS of a dense plasma. In the current literature involving heated, solid-density or compressed targets [83–87], the working assumption that $n_e = Z_f n_i$ has been used to infer Chihara's Z_f from the relative strengths of the first two XRTS terms in (42), or from the electron density that the measured position of a plasmon feature yields. Some of these experiments have shown certain orbital-based MIS values to be in reasonable agreement with data for plasmas at varying temperatures, while Saha-type MIS values underestimate the inferred degree of ionization at low temperatures. This is expected, since ionization based on a chemical picture does not include weakly bound or resonant-state contributions to the MIS. Even so, with what MIS computed by an orbital-based approach should one identify the Z_f extracted from XRTS? The quantity $\langle Z \rangle_{NPA}$ does define the ratio n_e/n_i of the background, uniform density plasma for that model and, as we have found, $Z^*_{Muze} \approx \langle Z \rangle_{NPA}$ under many conditions. On the other hand, according to Eqs. 29 and 39, both Z^*_{Muze} and $\langle Z \rangle_{NPA}$ include all positive-energy electrons but only that fraction of weakly bound, delocalized electrons existing outside the ion sphere. Moreover, orbital-based models include electrons in localized, resonant states of positive energy - states whose electrons probably participate differently in various plasma processes because they are not fully "free" [10, 54, 88].

As alternative strategies, one could identify Z_f as $\langle Z \rangle$ for some ion-sphere model. This would count just positive-energy electrons constituting the uniform background (cf. (20), but it would ignore, e.g., effects of the structure evident in the right panel of Fig. 4 and would exclude electrons in resonance states. Or, one could integrate the sum of "core" orbital terms (somehow defined) in (25) over the volume of the fundamental cell and then, by subtraction from Z_{nuc}, obtain a simple expression for Z_f that would correct the MIS for any diffuse, weakly bound states whose density partly lies within the ion sphere. In our view, such manipulation of DFT results to better match an experimentally inferred Z_f for high density, partially ionized matter is not particularly meaningful. A better formulation of XRTS may be needed here.

We illustrate these concepts by computing the ion static structure factor $S(k)$, which is proportional to the frequency integral of the quasielastic peak [48]. This part of the scattering cross section represents the portion of the scattered light that can probe ionic properties, such as the ion temperature T_i. Measuring the electron and ion temperatures separately is of paramount importance for many plasma studies. We consider normal solid den-

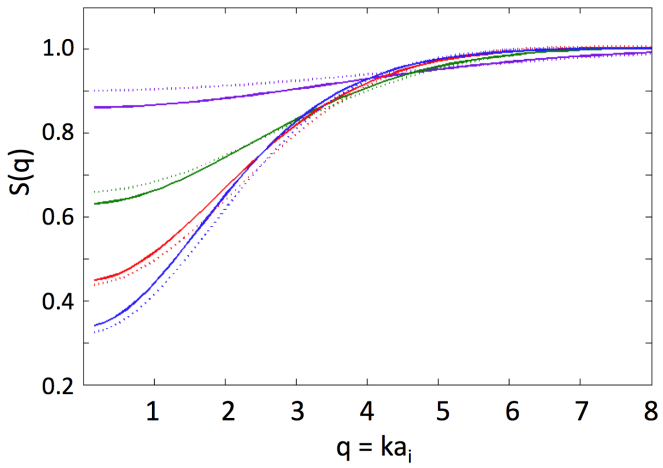

FIG. 12: (Color online) Structure factors for Be at $\rho = 1.85\text{g/cm}^3$ are shown for the four temperatures 5eV (top pair, purple), 10eV (first pair from top, green), 20eV (second pair from bottom, red), and 40eV (bottom pair, blue). The dashed lines correspond to the Z^* definition, while the solid lines correspond to the $\langle Z\rangle$ definition, here calculated using the TF model for the ionization and a Yukawa structure calculation. Due to ionization effects when $\Theta < 1$, the structure factors are very similar above $q = 3$ and provide no ion temperature information over this broad temperature range; however, temperature information is available at longer wavelengths.

sity Be and use a Yukawa model for the ion-ion interaction; the structure is computed using an MHNC approach [48]. Four temperatures, $T = 5, 10, 20, 40$eV, that span a wide degeneracy (Θ) range are studied, using only Thomas-Fermi results for $\langle Z\rangle$ and Z^*. The results are shown in Fig. 12.

We examine important features that emerge from this calculation. First, between $T = 5$eV and $T = 10$eV, the free electrons are moderately degenerate, and the ionic structure depends mainly on the ion temperature T_i, making that regime better for T_i measurements. Second, when $\Theta < 1$, there is atomic core excitation and ionization, which has two effects in the Yukawa model. Higher temperatures correspond to both larger charge states, and also to higher kinetic energies, which partially cancel in determining the Coulomb coupling parameter, yielding a smaller sensitivity to temperature in this temperature regime. Similarly, there is a partial cancellation in the screening parameter, since the electrons are hotter, but there are also more of them. This is particularly apparent in the comparison of the $T = 20$eV and $T = 40$eV cases, which differ by only as much as 30%. These are the basic features that ionization has on this portion of the XRTS spectrum.

Next consider the pairs of lines, in which the dashed and solids curves correspond to Z^* and $\langle Z\rangle$, respectively. The difference between the two ionization definitions is seen to be small, at most about 5%. This agreement can again be traced to the interplay between strong coupling and stronger screening so that the effective Coulomb coupling parameter (7) is weakened (when most models agree).

The factor $n(k)$ multiplying the ionic dynamic structure factor in (42) is usually a product of DFT procedures which require the density both in direct and reciprocal space. Using a DFT $n(k)$ for XRTS would be self-consistent since the same DFT calculation provides the MIS defining Z_f. This has not been the approach taken to date, but the effect of making this change in the analysis should be explored. Well beyond that, one could develop an "all electron" model of XRTS, in which a coupled, electron-ion DFT scheme is used to determine, self-consistently, all the electronic and ionic information necessary to interpret the scattering data. Such a model would involve treatment of plasma dynamics via time-dependent DFT [27], a topic undergoing rapid development [21, 28].

Future XRTS experiments could test details of orbital-based DFT calculations and better illuminate the role of weakly-bound and resonant states in the scattering process. Consider a mostly ionized plasma. Then, $n_c(k)$ represents very few electrons, and one can use XRTS measurements to study the density functional characterization of delocalized electrons. Conversely, when pressure ionization is modest, the use of XRTS to explore core electron issues is facilitated. By using different measurement angles (hence, probing different k-values), modulations in $n(k)$ caused by shell structure and/or continuum resonances and pseudogaps [63] might even be observable, although uncertainties in $S_{ii}(k,\omega)$ would need to be accounted for. In such investigation, plasmas where the distinction between core and free electrons is blurred (e.g., a case such as shown in Fig. 11) may be best. Another interesting XRTS study would be the change in plasma ionization across a predicted jump in the MIS for a case like in the left panel of Fig. 7 (for fixed density) or in Fig. 8 (for fixed temperature). Metal–nonmetal transitions are evident in electrical resistivity measurements of warm plasma under expansion, but the increase in resistivity with decreasing density is not as dramatic as the computed MIS behavior of ion sphere models would suggest (better overall agreement with electrical conductivity has been obtained from NPA-type calculations). These issues and complications notwithstanding, XRTS may be a better probe of ionization than integrated measurements of bulk transport properties, which do not generally distinguish the MIS effects on the scattering cross section from those on the number of charge carriers.

VI. SUMMARY AND FUTURE PROSPECTS

We have investigated the subject of ionization in dense plasmas, applying several formulations of DFT and several definitions of the MIS to the well-established notion of average atom models. Models based on an IS (i.e., Wigner-Seitz cell) do not yield a unique result for an

atom's MIS; models based on a larger CS do, although there is some latitude in how one deals with weakly bound electrons. We have discussed three MIS definitions, and compared numerical results of four DFT models, for the metals Be, Al, and Cu, over a wide range of conditions. These conditions, which represent plasmas having partial degeneracy and partial ionization, are accessible with a variety of experimental methods. We find very good agreement between the ion-sphere and correlation-sphere results for particular MIS definitions, but often see significant differences among other MIS-values. One way to obviate this issue is to cast a given problem in a purely "physical picture," which makes no reference to the MIS (i.e., uses all the electrons without finite-T pseudopotentials), but this remains impractical for many applications, and finite-T pseudopotentials [8, 9] will eventually play an important role, just as for $T = 0$ applications.

By using the common framework of DFT, comparisons among models and involving specific physics issues could be made unambiguously. We considered both OFDFT (finite-temperature TF) and orbital-based (KS) models. Also, we explored the importance of including an LDA exchange-correlation potential that is accurate at all relevant temperatures and densities [68]. Lastly, using the neutral pseudo-atom model we examined consequences of employing a fundamental cell larger than the ion sphere. Some of our key findings include:

- Under most conditions explored, there is excellent agreement between the IS and NPA based MIS-values defined as the integral of continuum electron density based on orbitals. However, the corresponding electron chemical potentials μ_e can differ considerably. Each model determines μ_e at the edge of its fundamental cell, but in orbital-based ion-sphere models the electron density there is not yet that of the interacting, *homogeneous* background. Larger differences between chemical potentials occur in plasmas with larger electron-ion coupling parameters, with a relationship that is roughly linear. The NPA μ_e, when modified for ion-subsystem effects as in Re. [8] may lead to closer agreement (or disagreement in some cases) with the IS values. This has not been investigated.

- In all cases, the (negative) exchange-correlation interaction serves to enhance binding and reduce the MIS; the same is true for the introduction of orbitals. But, their relative importance in IS models depends on the particular MIS definition in use. The relevance of a finite-T exchange-correlation potential is very clear.

- Because of the way resonance states are treated in orbital-based IS and NPA models, pressure ionization can cause large, jumps in Z^*. Such jumps are not present in either the chemical potential or in the ion-sphere MIS quantity $\langle Z \rangle$. These "jumps" physically correspond to rapid variations in the MIS, and such smoothed mean-Z values are obtainable in multi-state DFT models [8]. In fact, an abrupt change in the difference $\langle Z \rangle - Z^*$ when small changes in T or n_i is a good indicator of emergent structure in the low-energy sector of the continuum. The TF model fails to exhibit such behavior as it has no shell structure.

- From the discussion of X-ray Thomson scattering, it is evident that the measurement of ionization in WDM is far more problematic than it is in dilute plasmas, or solids and liquid metals, all of which, interestingly, have provided insights and techniques for the study of this complex regime. We agree with comments made by others [54] to the effect that, for IS models, the "best" MIS choice likely depends on just what phenomenon is being investigated. Even for CS models, where there is no MIS ambiguity, it should be remembered that an ion's charge state "is not the eigenvalue of any quantum operator" [89], and hence that one requires some physically motivated definition that sets the role of hopping electrons in a given situation [62]. However, even the temperature of a plasma is a property for which there is no direct quantum operator, and such properties are quite common in statistical physics. Hence, the lack of a quantum mechanical operator does not mean that a MIS cannot be extracted from suitable measurements like stopping power and electrical conductivity which include it. The temperature T of a plasma and the mean ionization Z can both be viewed as Langrange multipliers, where T is associated with the conservation of energy [90], while $\langle Z \rangle$ is a Lagrange multiplier associated with charge neutrality, as discussed in [60].

Progress motivated from this study should occur in a number of directions. There is in wide use a simple fit [54] to the TF value of $\langle Z \rangle$, computed without exchange-correlation. Because of the importance of this interaction at very high densities, as we have seen, and the ready availability of a fit for it (recall (15)), improved $\langle Z \rangle$ fits should be produced for a TFxc model; together with finite-temperature gradient corrections, a more accurate orbital-free model may result. Combining such a model with ionic structure [39, 41, 42] may yield a more accurate, all-electron model that includes self-consistent ionic correlations. The notion of an average atom with a definite MIS provides a simple one-parameter, finite-temperature pseudo-potential for describing ions in plasmas; determining, for example, ion-ion dynamic structure factors using more accurate ionic models could involve, e.g., atomic shells of specified radii and well depths [8]. A more accurate pseudo-potential is expected to be particularly important in plasmas having heavy ions with many bound electrons, and a comprehensive set of orbital-based DFT calculations would provide these pseudo-potential parameters, as already done in [8] for

Al ions in plasmas. Finally, extending comparative studies like the present one to plasmas with mixtures of elements is attractive.

Finally, we conclude by returning to the issue of which MIS is optimal for a given problem. In a study of dense plasma viscosity [91], strong sensitivity to the choice of the MIS was found. For such a problem one seeks the best effective ion-ion interaction potential, which is not easily tied to any of the MIS quantities we have considered, except perhpas those from coupled-CS models [92]. For electron-ion physics, measurements of the electrical conductivity can be used to deduce the most appropriate MIS [80]. In purely theoretical treatments, it is also possible to decide among several choices of the MIS through thermodynamic self-consistency arguments [14].

Acknowledgments– The work of MSM was supported by a research contract to Los Alamos National Laboratory from Lawrence Livermore National Laboratory. The work of JW was supported by research contracts to the University of Pittsburgh from Lawrence Livermore National Laboratory. The work of MSM and JW was part of the Cimarron Collaboration based at Lawrence Livermore National Laboratory. The Cimarron project is a combined theoretical, computational and experimental effort to understand the micro-physics of hot, dense burning plasmas. The work of SBH was performed in part under the auspices of the U.S. Department of Energy by Lawrence Livermore National Laboratory under Contract DE-AC52-07NA27344 and supported in part by Sandia, a multi-program laboratory operated by Sandia Corporation, a Lockheed Martin Company, for the U.S. Department of Energy under Contract No. DE-AC04-94AL85000. We wish to thank several colleagues for comments and advice received during the course of this collaboration, including especially Brian Wilson and Stephen Libby. Fianlly, we would also like to thank one of the referees for greatly improving this manuscript. This is document number LA-UR-13-23400.

[1] D. Salzmann, Atomic Physics in Hot Plasmas, Oxford U. Press, Oxford, 1998.
[2] H.-K. Chung et al., High Energy Density Physics **1** 3 (2005) .
[3] L. Spitzer, Jr., Physics of Fully Ionized Gases, Wiley Interscience, New York, 1962.
[4] Ya.B. Zeldovich, Yu.P. Raizer, Physics of Shock Waves and High-Temperature Hydrodynamic Phenomena, Ch. III, Dover, Mineola, N.Y., 2002.
[5] S. Atzeni, J. Meyer-ter-vehn, Physics of Inertial Fusion, Ch. 10, Clarendon, Oxford, 2004.
[6] J. Weisheit, M.S. Murillo, in Springer Handbook of Atomic, Molecular, Optical Physics, Ch. 86, ed. G.F.W. Drake, Springer, New York, 2006.
[7] E. Nardi et al., Phys. Rev. E **57** 4693 (1998).
[8] F. Perrot, M.W.C. Dharma-wardana, Phys. Rev. E **52** 5352 (1995).
[9] M. W. C. Dharma-wardana, Phys. Rev. E **73** 036401 (2006).
[10] D. Kremp, M. Schlanges, W.-D. Kraeft, Quantum Statistics of Nonideal Plasmas, Springer, Berlin, 2005.
[11] D.G. Hummer and D. Mihalas, Astrophys. J. **331** 794 (1988)
[12] F. J. Rogers and Carlo Iglesias, Science, **263** 50 (1994).
[13] F.J. Rogers, Phys. Plasmas **7** 51 (2000).
[14] T. Blenski, B. Cichocki, Phys. Rev. E **75** 056402 (2007) .
[15] G. Massacrier, J. Quant. Spectrosc. Radiat. Transfer **51** 221 (1994) .
[16] B.F. Rozsnyai, Phys. Rev. A **5** (1972) 1137.
[17] D. A. Liberman, Phys. Rev. B **20** 4891 (1979).
[18] P. Hohenberg and W. Kohn, Phys. Rev. B **136**, 864 (1964)
[19] W. Kohn, L. J. Sham, Phys. Rev. **140** A1133 (1965).
[20] E.K.U. Gross, R.M. Dreizler, eds., Density Functional Theory, Plenum, (1995).
[21] R. G. Parr and W. Yang, Density-Functional Theory of Atoms and Molecules, Oxford U. Press, New York, 1989.
[22] P. Wang, T.M. Mehlhorn, J.J. MacFarlane, Phys. Plasmas **5** 2977 (1998).
[23] M.W.C. Dharma-wardana, F. Perrot, Phys. Rev. E **58** 3705 (1998) .
[24] M.S. Murillo and M.W.C. Dharma-wardana, Phys. Rev. Lett. **100** 205005 (2008).
[25] F. Perrot and M. W. C. Dharma-wardana, Phys. Rev. A **33**, 33033313 (1986)
[26] J. Marten, C. Toepffer, Eur. Phys. J. D **29** 397 (2004).
[27] F. Grimaldi, A. Grimaldi-Lecourt, and M.W.C. Dharma-wardana, Phys. Rev. A **32** 1063 (1985)
[28] M.A.L. Marques and E.K.U. Gross, Ann. Rev. Phys. Chem. **55** 427 (2004).
[29] R. Kubo, M. Toda, N. Hashitsume, Statistical Physics II, 2ed, Ch. IV, Springer-Verlag, Berlin 1991.
[30] J.M. Ziman, Principles of the Theory of Solids, 2ed, Cambridge U. Press, Cambridge, 1972.
[31] W.R. Johnson, C. Guet, and G.F. Bertsch, J. Quant. Spectrosc. Rad. Trans. **99** 327 (1006).
[32] D. Marx and J. Hutter, Ab Initio Molecular Dynamics: Basic Theory and Advanced Methods, Cambridge University Press, 2009.
[33] J.-F. Danel, L. Kazandjian, G. Zerah, Phys. Rev. E **85**, 066701 (2012).
[34] C. Wang, X. T. He, and P. Zhang, Phys. Plasmas **19**, 042702 (2012).
[35] J.-F. Danel, L. Kazandjian, G. Zerah, Phys. Rev. E **79**, 066408 (2009).
[36] J.-D. Chai and D.D. Weeks, Phys. Rev. B **75** 205122 (2007) .
[37] M. Foley and P. A. Madden, Phys. Rev. B **53**, 10589 (1996).
[38] V. V. Karasiev, T. Sjostrom, and S. B. Trickey, Phys. Rev. B **86**, 115101 (2012).
[39] D. Ofer, E. Nardi, Y. Rosenfeld, Phys. Rev. A **38** 5801 (1998).
[40] W. Zakowicz, I.J. Feng, R.H. Pratt, J. Quant. Spectrosc. Radiat. Transfer **27** (1982) 329.
[41] H. Xu and J.-P. Hansen, Phys. Rev. E **57**, 211 (1998).
[42] J. A. Anta and A. A. Louis, Phys. Rev. B **61**, 11400

(2000).
[43] M. W. C Dharma-wardana and M. S. Murillo, Phys. Rev. E **77**, 026401 (2008).
[44] S. Ichimaru, Statistical Plasma Physics II, Addison-Wesley, Reading, MA, 1994.
[45] M.S. Murillo, Phys. Plasmas **11** 2964 (2004).
[46] M. W. C. Dharma-wardana and F. Perrot, Phys. Rev. Lett. **84** 959 (2000).
[47] C. Bulutay and B. Tanatar, Phys. Rev. B **65**, 195116 (2002)
[48] M. S. Murillo, Phys. Rev. E **81**, 036403 (2010).
[49] B. F. Rozsnyai et al., Phys. Letters A **291** 226 (2001).
[50] R. W. Lee et al., Laser and Particle Beams, **20** 527 (2002) .
[51] G. Gregori et al., Contrib. Plasma Phys. **45** 284(2005).
[52] A. Ng et al., Laser and Particle Beams **23** 527 (2005).
[53] E. Nardi et al., Laser and Particle Beams **24** 131 (2006).
[54] R. M. More, Adv. Atomic Molec. Physics **21** 305 (1985).
[55] S. Eliezer, A. Ghatak, H. Hora, An Introduction to Equation of State, Cambridge U. Press, Cambridge, UK, 1986.
[56] R. P. Feynman, N. Metropolis, E. Teller, Phys. Rev. **75** 1561 (1949) .
[57] S. B. Hansen et al., Phys. Rev. E **72** 036408 (2005).
[58] B. Wilson et al., J. Quant. Spectrosc. Radiat. Transfer **99** 658 (2006).
[59] M. Penicaud, J. Phys.: Condensed Matter **21** (2009) 095409.
[60] M. W. C. Dharma-wardana, F. Perrot, Phys. Rev. A **26** 2096 (1982).
[61] F. Perrot, Phys. Rev. A **42** 4871 (1990).
[62] M. W. C. Dharma-wardana, F. Perrot, Phys. Rev. A **45** 5883 (1992).
[63] M.S. Murillo, J.C. Weisheit, J. Quant. Spectrosc. Radiat. Transfer, **54** 271 (1995).
[64] C. Blancard, G. Faussurier, Phys. Rev. E **69** 016409 (2004).
[65] J. Chihara, Progress of Theoretical Physics, **59** (1978) 76; J. Kihara and S. Kambayashi, J. Phys: Condens. matter **6** 10221 (1994).
[66] G. Ortiz and P. Ballone, Phys. Rev. B **50 1391** (1994)
[67] M. W. C. Dharma-wardana, R.Taylor, J.Phys. C **14** 629 (1981).
[68] F. Perrot, M. W. C. Dharma-wardana, Phys. Rev. A **30** 2619 (1984).
[69] F. Perrot, M. W. C. Dharma-wardana, Phys. Rev. B **62** 16536 (2000) Erratum **67**, 79901 (2003)
[70] R. G. Dandrea, N. W. Ashcroft, and A. E. Carlsson, Phys. Rev. B **34** 2097 (1987)
[71] D. G. Kanhere, P. V. Panat A. K. Rajagopal and J. Callaway, Phys. Rev. A **33**, 490497 (1986)
[72] S. Ichimaru, H. Iyetomi, S. Tanaka, Phys. Reports **149** 91 (1987).
[73] B. Ritchie, Phys. Rev. B **75** 052101 (2007).
[74] H. Szichman, Phys. Rev. B **43** 6094 (1991).
[75] E. Cappelluti, L. Delle Site, Physica A **303** 481 (2002).
[76] R. M. More et al., Phys. Fluids **31** 3059 (1988).
[77] P. Fromy, C. Deutsch, G. Maynard, Phys. Plasmas **3** 714 (1996).
[78] N.D. Mermin, Phys. Rev. **137** A1441 (1965).
[79] W. Kohn and C. Majumdar, Phys. Rev. **138** A1617 (1965).
[80] P.A. Sterne et al., High Energy Density Phys. **3** 278 (2007).
[81] T. Blenski and K. Ishikawa, Phys. Rev. E **51** 4869 (1995).
[82] G. Faussurier, P. L. Silvestrelli, C. Blancard, High Energy Density Physics **5** (2009) 74.
[83] A. L. Kritcher et al., Science **322** 69 (2008).
[84] J. Chihara, J. Physics: Condensed Matter **12** 231 (2000).
[85] G. Gregori,et al., Phys. Rev. E **67** 026412 (2003).
[86] G. Gregori,et al., Phys. Plasmas **11** 2754 (2004).
[87] S.H. Glenzer et al., Phys. Rev. Letters **98** 065002 (2007).
[88] F. Perrot, M.W.C. Dharma-wardana, Intl. J. Thermophysics, **20** 1299 (1999).
[89] F. Perrot, Phys. Rev. A **47** 570 (1993).
[90] M. W. C. Dharma-wardana and F. Perrot, Phys. Rev. E **63** 069901 (2001).
[91] M. S. Murillo, High Energy Density Physics **4** 49 (2008).
[92] F. Nadin, G. Jacucci and M.W.C. Dharma-wardana, Phys. Rev. A **37**, 1025-1028 (1988)